AD-A096 079 IOWA UNIV IOWA CITY DEPT OF PHYSICS AND ASTRONOMY F/G 3/2
PLASMAS IN SATURN'S MAGNETOSPHERE,(U)
APR 80 L A FRANK, B G BUREK, K L ACKERSON
UNCLASSIFIED U OF IOWA 80-12 NL

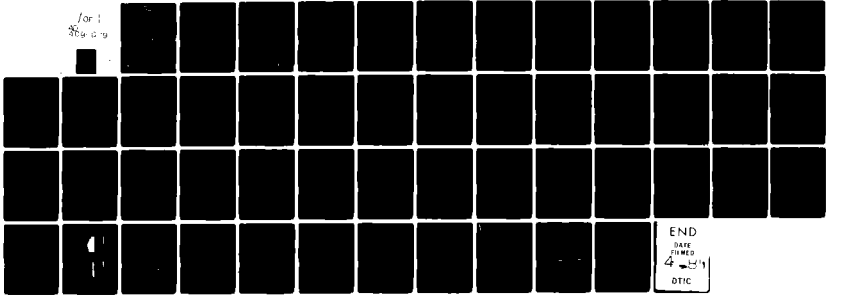

LEVEL II

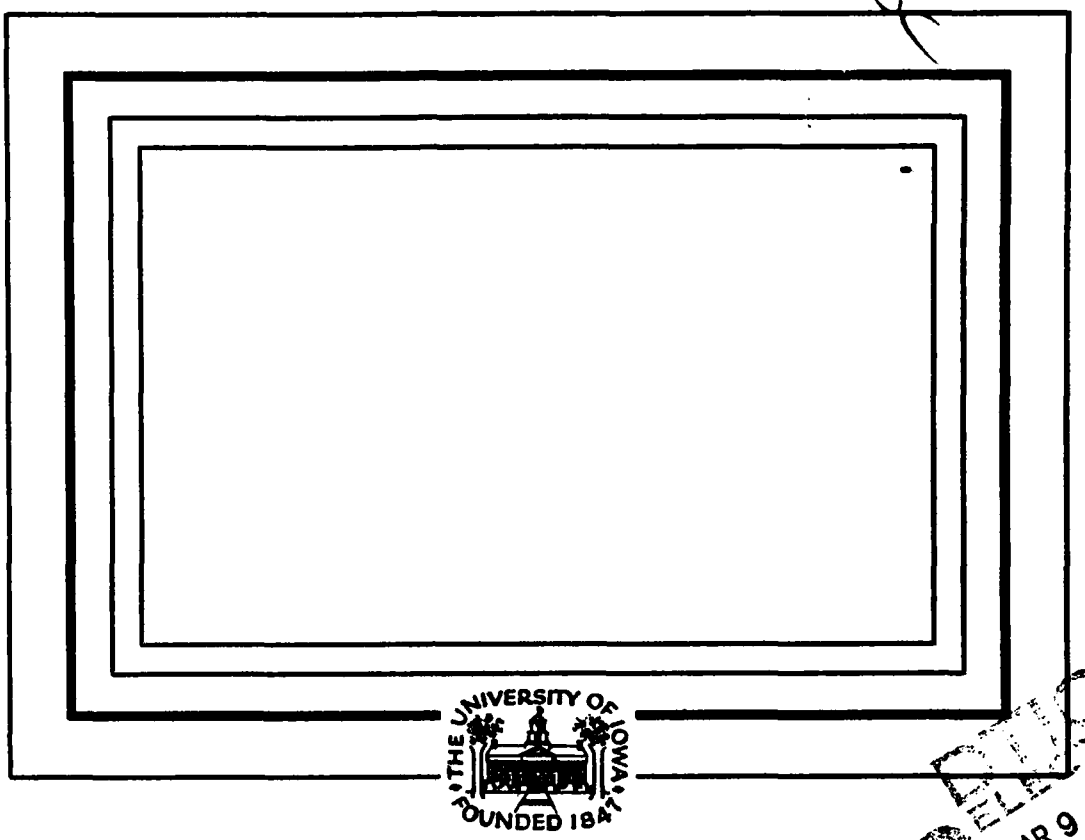

Department of Physics and Astronomy

THE UNIVERSITY OF IOWA

Iowa City, Iowa 52242

(1)

(6) PLASMAS IN

SATURN'S MAGNETOSPHERE

by

(10) L. A. Frank[1] B. G. Burek[1]

K. L. Ackerson[1] J. H. Wolfe[2]

and J. D. Mihalov[2]

(11) April 1980

(12) 51 L

Department of Physics and Astronomy
The University of Iowa
Iowa City, Iowa 52242

Submitted for publication to Journal of Geophysical Research

[1]Department of Physics and Astronomy, The University of Iowa, Iowa City, Iowa 52242

[2]Space Science Division, NASA/Ames Research Center, Moffett Field, California 94035

Abstract

The solar wind plasma analyzer on board Pioneer 11 provides first observations of low-energy positive ions in the magnetosphere of Saturn. Measurable intensities of ions within the energy-per-unit charge (E/Q) range 100 eV to 8 keV are present over the planetocentric radial distance range $\sim$ 4 R_S to 16 R_S in the dayside magnetosphere. The plasmas are found to be rigidly corotating with the planet out to distances of at least 10 R_S. At radial distances beyond 10 R_S, the bulk flows appear to be in the corotation direction but with lesser speeds than those expected from rigid corotation. At radial distances beyond the orbit of Rhea at 8.8 R_S, the dominant ions are most likely protons and the corresponding typical densities and temperatures are 0.5 cm^{-3} and 10^6 °K, respectively, with substantial fluctuations. Identification of the mass-per-unit charge (M/Q) of the dominant ion species is possible in certain regions of Saturn's magnetosphere via the angular distributions of positive ions. A large torus of oxygen ions is located inside the orbit of Rhea and the densities are $\gtrsim$ 10 cm^{-3} over the radial distance range $\sim$ 4 R_S to 7.5 R_S. Density maxima appear at the orbits of Dione and Tethys where oxygen ion densities are $\sim$ 50 cm^{-3}. The dominant oxygen charge states are O^{2+} and O^{3+} in the radial distance ranges $\sim$ 4 R_S to 7 R_S and 7 R_S to 8 R_S, respectively. The observations are suggestive of a decrease of ion energies to values less than the instrument energy threshold of E/Q = 100 eV at the apparent inward edge of the torus at 4 R_S. Ion temperatures increase rapidly from $\sim$ 2 X 10^5 °K at 4 R_S to 5 X 10^6 °K at 7.3 R_S. It is concluded that the most likely source of these plasmas is the photodissociation of water frost on the surface of the ring material with subsequent ionization of the products and radially outward diffusion. The sources associated with the satellites Dione and Tethys are probably of lesser strength. The presence of this plasma torus is expected to have a large influence on the dynamics of Saturn's magnetosphere since the pressure ratio β of these plasmas approaches unity at radial distances as close to the planet as 6.5 R_S. On the basis of these observational evidences it is anticipated that quasi-periodic outward flows of plasma, accompanied with a reconfiguration of the magnetosphere beyond $\sim$ 6.5 R_S, will occur in the local night sector in order to relieve the plasma pressure from accretion of plasma from the rings.

I. Introduction

Prior to the encounter of Saturn with Pioneer 11, in situ measurements show the existence of two planetary magnetospheres with great reservoirs of plasmas, those of earth and Jupiter. The sources and dynamics of these plasma regimes of the two planets greatly differ and both offer exciting, naturally-occurring laboratories with an abundance of plasma phenomena. The terrestrial plasma regimes, the plasma sheet and the ring current, are fed by both the solar wind and the earth's ionosphere. The dynamics of these regions are sensitively tuned to the state of the solar wind which supplies the energy for acceleration of these plasmas. No substantial effect on the overall dynamics or as a plasma source is exerted by the earth's moon. On the other hand, a principal body of plasma in the Jovian magnetosphere occupies a large torus in the vicinity of the orbit of the moon Io. The source of these plasmas is the sporadic volcanic activity of this satellite. The ion composition includes those of sulfur and oxygen as ionization products of sulfur dioxide. Plasma flows are dominated by the corotational electric fields generated by the short rotational periods and large magnetic fields associated with the planet. Although the ion densities within the torus are high, this plasma exhibits a relatively low ratio of plasma and magnetic field pressures, $\beta < 10^{-2}$, as compared to values of approximately unity within the terrestrial plasma sheet and outer ring current. With plasma measurements during the traversal of the Saturn magnetosphere with

Pioneer 11 a third magnetosphere with a large reservoir of plasma is found. The dominant ion species appears to be oxygen and these plasmas are located in a large torus encircling Saturn and engulfing the orbits of Dione and Tethys. Plasma motions are dominated by rigid corotational bulk flow. The ions appear to be the ionization products of water frost on the surfaces of the ring material and are transported radially outward and energized to form a large plasma torus. The dynamics of this plasma torus are likely to differ substantially from those of the Io torus since the torus surrounding Saturn is found to have remarkably high β values approaching unity at radial distances as small as $\sim 6\ R_S$. Thus the possibility exists that the source of plasma from photodissociation of water and subsequent ionization of the OH radical by electron impact with the ambient electron velocity distributions exceeds loss rates from radial diffusion, recombination and charge exchange, and provides a plasma pressure sufficiently large to disrupt the magnetosphere of Saturn. If so, Saturn's magnetosphere would be expected to experience a periodic, perhaps explosive release of plasmas from the torus. Preliminary results from observations of plasmas in Saturn's magnetosphere with Pioneer 11 are given previously by Wolfe et al. [1980]. We report here the results of an extensive analysis of these plasma measurements.

II. Observations

The measurements of positive ion velocity distributions within the magnetosphere of Saturn as reported here are gained with the high-resolution electrostatic analyzer of the Ames Research Center solar wind plasma instrumentation on board Pioneer 11. A description of this plasma instrument is given by Wolfe et al. [1974]. We summarize briefly several of the instrument characteristics directly pertinent to the present investigation. The high-resolution analyzer spans the energy-per-unit charge range of 100 eV $\leq$ E/Q $\leq$ 8 keV with an energy resolution $\Delta(E/Q)/(E/Q) \approx 0.07$ in 64 contiguous passbands. This electrostatic analyzer comprises quadrispherical plates and multiple sensors in order to provide measurements of the three-dimensional velocity distributions of positive ions within a conical field-of-view with half-angle 50.4° and centered along the spacecraft spin axis. Two of the sensors, all continuous-channel electron multipliers, are designed with significantly larger geometry factors relative to those of the main body of sensors which are dedicated to measurements of solar wind and magnetosheath plasmas. The larger geometry factors of these two sensors are intended to accommodate the hotter, quasi-isotropic plasmas typically found in planetary magnetospheres. Their fields-of-view are positioned at the edges ($\pm$ 50.4°) of the fan-shaped field-of-view of the high-resolution plasma analyzer. The spacecraft spin-axis is directed parallel to the central axis of this fan-shaped field-of-view, hence providing measurements of the angular distributions of positive ions

within a 50.4° cone as noted above. All of the plasma measurements reported here utilize the responses of one of the sensors with larger geometry factor and the center of its field-of-view of width 8° in cone angle lies at the surface of the effective conical field-of-view of the instrument. The trajectory of Pioneer 11 through Saturn's dayside magnetosphere and the orientation of the sensor's field-of-view are summarized in Figure 1. Our present analysis is limited to the inbound trajectory which is favorable for viewing in directions near the corotational flow vector; the geometry of the outbound trajectory positions the field-of-view at large angles, $\gtrsim$ 110°, to this bulk flow vector. The characteristic thermal speeds of the positive ions relative to the bulk flow speed are sufficiently small as to obviate a substantial study of plasmas along the outbound trajectory at radial distances $\lesssim$ 10 R_S (R_S, 1 Saturn radius = 60,000 km). The inbound trajectory as projected onto Saturn's equatorial plane is shown in the left-hand panel of Figure 1. Plasma observations for the period ~ 0000 to 1500 ERT (Earth Received Time of the telemetry signal) on September 1, 1979 are discussed in detail here. Definitive ion measurements are obtained over the radial distance range 4 R_S to 16 R_S. The magnetopause crossing occurs at 2209 ERT on August 31 at 17.3 R_S [Wolfe et al., 1980]. The trajectory lies close to the projections of the Saturn-to-sun and Saturn-to-earth vectors. The positions of four of Saturn's satellites are also shown for times corresponding to the spacecraft's crossing of their respective orbits. As shown in the right-hand panel of Figure 1, the spacecraft

spin axis is aligned along the spacecraft-to-earth vector. The axis of the field-of-view of sensor 1 is also shown along with the expected corotation velocity vectors at 5 R_S and 15 R_S. The field-of-view passes close, $\lesssim 25°$, to this corotation vector throughout this segment of the inbound trajectory. The responses of the sensor are accumulated for one-half spin period (1 spin period = 7.69 seconds) and subsequently telemetered. Corresponding directions of the axis of the sensor field-of-view are summarized in the bottom right-hand diagram of Figure 1. The spin phase angle $\phi = 0°$ occurs when this axis of the field-of-view is parallel to the ecliptic and ascending toward the north ecliptic pole. Responses of the sensor are accumulated for two half spins $\pi/2 \leq \phi < 3\pi/2$ and $3\pi/2 \leq \phi < 2\pi$, $0 \leq \phi < \pi/2$, hereafter referred to as angular sectors $\phi' = \pi/2$ and $\phi' = 3\pi/2$, respectively. These measurements of angular distributions are used in the present analysis for identification of ion species, or more specifically, mass-per-unit charge, M/Q. The angular sector $\phi' = \pi/2$ generally views toward the corotational bulk flow vector. For the measurements of positive ions in the dayside magnetosphere the instrument operating mode constitutes sampling the half-spin sectors $\phi' = \pi/2$ and $\phi' = 3\pi/2$ with alternate energy passbands such that samples of ion intensities are available for 32 energy passbands for each of the two sectors. The temporal resolution (instrument cycle time) for gaining each such series of measurements at Saturn is 780 seconds.

The responses of the plasma analyzer (sensor 1) to positive ions as functions of energy (E/Q) and time on September 1, 1979 are shown in

the color spectrograms of Plate 1. These responses are plotted as functions of the energy in units of eV and the Universal Time for reception of the telemetry signal at earth (also ERT), and are color-coded according to the color bar on the right-hand side of the spectrograms. The color bar is calibrated in units of the logarithm base 10 of the sensor responses accumulated during a half-spin of the spacecraft. The upper spectrogram corresponds to the spin sector $\phi' = \pi/2$ (generally viewing into the corotation vector), and the bottom spectrogram shows responses for the sector $\phi' = 3\pi/2$. The larger sensor responses for the spectrogram for sector $\phi' = \pi/2$ are indicative of the corotation of plasmas in Saturn's magnetosphere. During the period 0000 to 0800 ERT the intensities of positive ions are relatively low, and correspond to densities $\lesssim 1\ cm^{-3}$, as contrasted to those intensities encountered deeper within the magnetosphere for the period ~ 0800 to 1500 ERT. The high responses after 1500 ERT are attributable to background rates due to energetic charged particles. The instrument is commanded off for the period ~ 1630 to 2330 ERT. Periapsis is located at 1.35 R_S and occurs at 1757 ERT. Significant background responses can also be seen in the spectrograms for the period ~ 0900 to 1500 ERT as evidenced by the lack of modulation of sensor responses with energy (plate voltage) at energies $\gtrsim 3$ keV. These background rates are subtracted from the sensor responses at lower energies before the velocity distribution functions are calculated. For examples, the background counts per accumulation period are 12 and 122 at 0943 ERT and 1416 ERT, respectively. There are approximately 60 complete measurements of ion energy spectra, with responses above background rates, for the observations shown in Plate 1.

Analysis of the instrument responses proceeds by converting these responses to phase space densities n(V) for each of the two sectors and by assuming that M/Q = 1, 2, 4, 8 or 16. A Maxwellian distribution with corotational bulk flow velocity $\vec{V}_o$, density N and temperature T is employed to find a best nonlinear least squares fit for each of the above species. Details of this computation are given in the Appendix. In general when observations are available for both angular sectors $\phi' = \pi/2$ and $\phi' = 3\pi/2$ only one of the above species provides a good fit. Our following discussion presents detailed results of these computations which are central to the determinations of N and T and to the identification of the species. For the observations in the outer magnetosphere for the period ~ 0000 to 0800 ERT, i.e., ~ 16 R_S to 10 R_S, few good fits to a corotating plasma of any species are acquired. However, all velocity distributions which did provide a good fit, e.g., at 0431 and 0602 ERT, are identified as M/Q = 1, or H^+. It is likely that the outer magnetosphere is not rigidly corotating at these larger radial distances. A further analysis assumes that the ions are H^+ and that the bulk flow $\vec{V}_B$ is in the same direction as corotational flow but with a fraction of the expected rigid corotation speed. Again a nonlinear least squares fit was employed for each value of V_B to find the best fit to the observed velocity distribution. An example of these results is shown in Figure 2 for the velocity distribution acquired at 0024 ERT (15.7 R_S). Statistical uncertainties in the observed n(V) are less than $\pm$ 20% for this and later such series of measurements. The two angular sectors $\phi' = \pi/2$ and $\phi' = 3\pi/2$

are noted along the abscissa. A bulk speed of 0.5 V_o with T = 1.2 X 10^6 °K and N = 0.19 cm^{-3} provides a good fit to the measurements if the high-speed tails of the distribution at V > 3 X 10^7 cm/sec are excluded. On the other hand, not all of the observed velocity distributions in the outer magnetosphere can be fit with a Maxwellian distribution flowing with a fraction of the corotation speed. An example of a poor fit is shown for 0117 ERT in Figure 3. Each velocity distribution provides a reasonable fit to the angular sector $\phi' = \pi/2$, excluding the high-speed tail, but no apparent fit for the complementary sector $\phi' = 3\pi/2$ is found. There are three immediate possibilities for the origins of this poor fit: temporal variations, a non-Maxwellian velocity distribution or missing telemetry for the sector $\phi' = 3\pi/2$ in the velocity range ~ 1.8 to 2.8 X 10^7 cm/sec. However, approximately 40% of the observed velocity distributions with usable measurements for both angular sectors can be fit with such a Maxwellian with bulk speed V_B and directed along the corotational vector. This flow speed ranged from 0.3 to 0.8 V_o. Rigid corotation of a hydrogen plasma is observed later during the period 0800 to 1010 ERT which corresponds to a radial distance range of 10 R_s to 8.2 R_s. A substantial fraction of these velocity distributions are well fit with the computed distributions for $V_B = V_o$. Thus the plasmas within Saturn's magnetosphere are rigidly corotating with the planet at radial distances $\lesssim$ 10 R_s. Beyond 10 to 12 R_s the plasma bulk velocities appear to be along the corotation direction but with a fraction, 0.3 to 0.8, of the expected corotation speed.

For the period after the encounter with corotating hydrogen plasmas, i.e., after 1010 ERT, heavy ions and increasing densities are detected with the plasma instrument (see Plate 1). Two zones which are each distinguished by differing M/Q values for the ions are found. These two zones span the periods 1010 to 1130 ERT (8.2 R_S to 7.1 R_S) and 1130 to 1442 ERT (7.1 R_S to 4.1 R_S), respectively. Examples for the best fits to the observed velocity distributions for various assumed M/Q values are shown in Figures 4 and 5. Best fits for four ion species for the ion velocity distributions observed at 1127 ERT (7.1 R_S) are shown in Figure 4. It should be noted that the two velocity distributions corresponding to sectors $\phi' = \pi/2$ and $\phi' = 3\pi/2$ provide a very sensitive measure of the M/Q of the ion species. The density N and temperature T for each best fit is also given in Figure 4. Poor fits to the observed velocity distributions are yielded by M/Q values of 1 (H^+) and 16 (O^+) whereas considerably better, but not perfect fits are provided by M/Q values of 4 (He^+) and 8 (O^{2+}). Inspection of these latter two fits yields an assessment of the M/Q of the dominant species as 5 to 6 amu/unit charge with a density $N \simeq 10$ cm^{-3} and temperature $T \simeq 1.5 \times 10^6$ °K. An example of similar calculations for the second ion zone at lesser radial distances is given in Figure 5. This velocity distribution at 1219 ERT (6.4 R_S) is very well fit with an ion distribution with M/Q = 8, N = 40.8 cm^{-3} and T = 1.6×10^6 °K with the exception of the high-speed tails at $V \gtrsim 1.2 \times 10^7$ cm/sec. We note here the known presence of water frost on the satellites Dione and Tethys [Morrison et al., 1976; Fink et al., 1976] which are embedded in this large plasma torus, and on the nearby

ring material [Pilcher et al., 1970; Kuiper et al., 1970], and identify the ions with M/Q ≈ 5-6 as O^{3+} (M/Q ≈ 5.3) and those with M/Q ≈ 8 as O^{2+}. For the time period 1245 to 1442 ERT (6.0 R_S to 4.1 R_S), the plasma has cooled to the extent that velocity distributions cannot be determined for the angular sector $\phi' = 3\pi/2$ (cf. Plate 1). Without this complementary angular measurement, the identification of ion species becomes less certain since it relies upon the velocity distributions for sector $\phi' = \pi/2$ only. An example of observations of ion velocity distributions in these cooler plasmas is shown in Figure 6, together with best fits to corotating Maxwellian distributions for several ions. The fit for O^+ is poor since no peak in the velocity distribution is observed and hence ions with $M/Q \gtrsim 16$ can be eliminated as possibilities. Reasonably good fits are obtained for the M/Q range ~ 4 to 8 but those for M/Q = 1 and 2 are poorer since a considerable fraction of the observed densities fall below the best-fit Maxwellian distributions. These comparisons are consistent, but not exclusively supportive, of our conclusion that the ions within the radial distance range 7.1 R_S to 4.1 R_S are O^{2+}. At lesser radial distances than 4.1 R_S, no responses of the plasma instrument to positive ions in the energy range 100 eV $\leq$ E/Q $\leq$ 8 keV are discernible (cf. spectrograms of Plate 1 for times later than 1442 ERT). However, the rapidly decreasing average ion energy with decreasing radial distance for this time period as clearly evidenced in the top spectrogram of Plate 1 is suggestive of a decrease of the ion average energy to values below the threshold of the instrument at 100 eV-per-unit charge.

We note again the substantial high-speed tails of several of the velocity distributions presented here, for example, those for the velocity distribution at $V \gtrsim 1.2 \times 10^7$ cm/sec in the lower left-hand panel of Figure 5. The dominant ion species is O^{2+} in this region. On the other hand, the densities within the high-speed tails are sufficiently large to encourage an attempt at identification of the associated ion species. The velocity distribution observed at 1206 ERT (6.6 R_S) is chosen here for analysis. The dominant ion is also O^{2+} with density and temperature, 26.8 cm^{-3} and 1.6×10^6 °K, respectively. The results of calculations for best-fit corotating Maxwellians for several ion species are summarized in Figure 7. No reasonable fits are obtained for M = 1, 2 or 16 amu thus eliminating H^+ and O^+ as the secondary ion component that appears in the velocity distribution. The best fits for M = 4 and 8 amu are both sufficiently good that O^{2+} (M/Q = 8) and O^{3+} (M/Q = 5.3) cannot be distinguished, although M = 5-6 fit (not shown) provides a somewhat better fit than M = 4 or 8. The corresponding temperatures and densities are 4.8×10^6 °K and 6.9 cm^{-3}, respectively, if the ions are O^{2+}, and 8.1×10^6 °K and 6.9 cm^{-3} for O^{3+}. (See Appendix for treatment of cases for Q > 1.) Thus the second ion component is substantial in density relative to that of the O^{2+} for this example and is probably either a hotter velocity distribution of O^{2+} or a coexisting O^{3+} ion plasma. A reasonable upper bound to the H^+ densities within the energy range 100 eV to 8 keV at this position in the plasma torus is ~ 5 cm^{-3}.

The individual measurements of positive ion spectra, a total of approximately 60 such observations, were each subjected to the same extensive nonlinear least square fit as that for the examples given above. These examples qualitatively cover the entire range of types of positive-ion velocity distributions that are observed in the dayside magnetosphere. A summary of the complete series of observations is given in Figure 8 which displays ion density, dominant ion species and ion temperature as functions of planetocentric radial distance. Ion densities over the radial distances ~ 9 to 16 R_s, and outside the orbit of Rhea, generally ranged from ~ 0.2 to 0.5 cm^{-3}. These densities monotonically increase from 0.6 cm^{-3} at Rhea's orbit to 45 cm^{-3} at the orbit of Dione. Densities are ~ 10 to 50 cm^{-3} in the plasma torus at 4.2 to 7.5 R_s. Two density maxima appear to be associated with Tethys and Dione. The ion density decreases rapidly with decreasing radial distance to instrument threshold values just outside the orbit of Enceladus. The center panel of Figure 8 shows our best evaluation of ion species as per the procedures discussed above. Periods for which there are (1) angular distributions with good fits to a corotating Maxwellian distribution, (2) angular distributions with poor fits to rigid corotation and (3) no available angular distributions are specifically designated in Figure 8. Our interpretation of the dominant ion species is also shown: O^{2+} at 4.1 to 7.1 R_s, O^{3+} at 7.1 to 8.2 R_s, and H^+ at 8.2 to 16 R_s, subject to the assumptions of our analysis as presented above for specific examples. Ion temperatures outside the orbit of Rhea fluctuate greatly and range from ~ 3 X 10^5 to 5 X 10^6 °K. A maximum in the ion temperature of ~ 6 X

10^6 °K is centered at 9.8 R_S. Inside the orbit of Rhea, ion temperatures monotonically increase to a maximum temperature of 5 X 10^6 °K at 7.3 R_S and subsequently decrease with decreasing radial distance to ~ 2.5 X 10^5 °K at 4.1 R_S just outside the orbit of Enceladus. The ion temperatures in this latter region at 4.1 to 7.3 R_S exhibit an extremely steep gradient and are roughly proportional to R^6. Overall an inspection of Figure 8 shows that the major plasma feature of the dayside magnetosphere is the large plasma torus of heavy ions, dominantly O^{2+} and O^{3+}, at ~ 4 to 8 R_S.

Other remarkable features of the plasma torus are the magnitudes of the ion energy densities, ε, and the ratios of plasma and magnetic field pressures, β, at radial distances deep within Saturn's magnetosphere. These parameters are shown as functions of radial distance in Figure 9. The scale for ε, in units of ergs/cm^3, is given along the left-hand ordinate and for β, along the right-hand ordinate. Energy densities beyond the orbit of Rhea range from ~ 2 X 10^{-11} to 2 X 10^{-10} erg/cm^3. The corresponding β-values are 0.02 to 0.5. The pressure ratio β has been calculated using a centered dipole field with magnetic moment 0.2 gauss-R_S^3 [cf. Smith et al., 1980]. The actual fields at the larger radial distances near the magnetopause are somewhat greater than those calculated with this dipole field approximation, but will not qualitatively affect the relatively high values for β. There is a relative minimum in the values for β, 0.02, at 8.8 to 9.7 R_S just outside the orbit of Rhea. Maximum energy densities are positioned at ~ 6.0 to 7.9 R_S within the plasma torus and attain values as high as 1.1 X 10^{-8} ergs/cm^3 at Dione's

orbit. There is a more modest maximum of energy density, ~ 4 X 10^{-9} erg/cm^3, near the orbit of Tethys. The values for β are particularly high, > 0.2, over the radial distance range ~ 6.0 to 8.0 R_S and approach unity in the vicinity of 7.5 R_S. To this stress on the magnetic field must be added that due to the rapid corotation of the plasma. It appears likely that, in view of these large values for β and the nature of the mechanism that provides a continuous source of ions to the plasma torus, the magnetosphere of Saturn is marginally stable or unstable for confinement of torus plasmas at radial distances as close to the planet as 6.5 R_S.

III. Discussion

First measurements of plasmas, specifically low-energy positive ions, within Saturn's magnetosphere are reported. The observations are gained with an electrostatic analyzer that is intended for comprehensive determinations of the velocity distributions of solar wind ions and electrons. Positive ion intensities within the dayside magnetosphere are sufficiently large that clear, usable analyzer responses to these ions occur over a radial distance range of ~ 4 to 16 R_S. An electrostatic analyzer is incapable of determining the ion species: however, the observed corotation of the plasma allows an assessment of mass-per-unit-charge, M/Q, of the dominant ion species. The plasma is observed to rigidly corotate with the planet to planetocentric radial distances of ~ 10 R_S. Beyond 10 R_S the bulk flow speed varies and appears to be ~ 0.3 to 0.8 of the expected rigid corotation speed V_O, presumably due to viscous drag from the solar wind and/or mass loading from the magnetospheric plasmas. The dominant ion species beyond a radial distance of ~ 8 R_S appears to be H^+, subject to the conditions of the interpretation that are given in the previous discussion of results. Inside radial distances of 8 R_S, heavy ions with M/Q ~ 8 and 5-6, respectively, are detected within a large, relatively dense plasma torus surrounding Saturn. This plasma torus extends from ~ 4 R_S to 9 R_S and is approximately bounded by the orbits of Enceladus and Rhea. Peak ion densities within the plasma torus are ~ 50 cm^{-3}, whereas beyond the torus in the outer magnetosphere these densities are typically less by a factor of 100, or ~ 0.5 cm^{-3}. A maximum in ion temperature of ~ 5 X 10^6 °K in

the torus is located at ~ 7.5 R_S and a steep gradient of ion temperatures occurs with decreasing radial distance to 4.1 R_S where the temperature is 2.5 X 10^5 °K. The ratios of plasma pressure to magnetic field pressure, β, are remarkably high and are near values of unity as deep within Saturn's magnetosphere as 6.5 R_S. This situation appears to indicate that Saturn's magnetospheric configuration is marginally stable or unstable at these radial distances and beyond. It is suggested that this large plasma pressure is periodically relieved, perhaps with a dramatic outflow of plasma, in the tailward sector of the magnetosphere where magnetic stresses are less likely to contain these plasmas. Two distinct maxima of ion densities occur within the plasma torus, one each at the orbits of Dione and Tethys. In lieu of another known source of heavy ions in this region, with the possible exception of the E ring, we conclude that the source for the plasma torus is Saturn's rings or the satellites Dione and Tethys.

There are two principal measurements of other phenomena in the dayside magnetosphere with Pioneer 11, that are directly correlated at first inspection with the presence of the plasma torus: a depression in magnetic field magnitudes below those values expected for Saturn's dipole at ~ 5 R_S to 10 R_S [Smith et al., 1980] and a severe decrease of energetic proton intensities with energies $\gtrsim$ 100 keV at the outer edge of the plasma torus [Van Allen et al., 1980a; Simpson et al., 1980; Trainor et al., 1980; Fillius et al., 1980]. The magnetic field depression is presumably related to the diamagnetic effects of the high-β torus plasma. For example, this decrease in the magnetic field intensity is ~ 5 γ at 8 R_S relative to the expected centered-dipole total field of 41 γ [Smith

et al., 1980]. Between the radial distances of 10 R_S and 17 R_S (magnetopause) the measured fields exceed the dipole values by ~ 5 γ. A detailed calculation of the magnetic perturbations due to the observed ion energy densities, including the effects of the magnetopause current system, will be undertaken as a future effort in order to show that the measured magnetic fields are consistent in detail with the plasma distributions reported here. Decreases in energetic proton intensities are not as easily identified with the presence of the plasma. For example, the loss of energetic protons may be associated with strong pitch-angle scattering into Saturn's ionosphere by wave-particle interactions, or may be the result of charge-exchange with an ambient, diffuse atomic hydrogen gas. Observations of pitch-angle distributions of the plasmas and of plasma waves are necessary to resolve this mechanism unambiguously. Such measurements are not available with the Pioneer 11 spacecraft. Wave-particle interactions should be abundant in such high-β plasmas if the earth's plasma sheet is used as a guide [cf. Gurnett et al., 1976]. The investigators for the energetic particle instruments cited above also report remarkable asymmetries in the intensities of both energetic protons and electrons for the inbound and outbound segments of the Pioneer 11 trajectory at radial distances ~ 4 to 10 R_S where significant azimuthal drift asymmetries and large effects from solar wind perturbations are not expected. We believe that this asymmetry is probably the signature of a large temporal change in this part of Saturn's magnetosphere, which is associated with a substantial outflow of torus plasmas between the periods of the inbound and outbound trajectories as the solar wind pressure on the magnetosphere decreased [Wolfe, et al., 1980] and internal magnetic stresses lessened.

Rigid corotation of the plasma allows identification of the M/Q of the dominant species within the torus: ~ 8 at 4.1 to 7.1 R_S, and ~ 5 at 7.1 to 8.2 R_S. To specifically identify the positive ions we are guided by observations of water frost or ice on the surfaces of Dione and Tethys and on the ring material and conclude that the species with M/Q ~ 8 is O^{2+}, and that with M/Q ~ 5 is O^{3+}. Except at the outer edge of the torus at ~ 8.2 to 8.6 R_S, the anticipated ion H^+ from photodissociation of H_2O was not observed in the torus. A corresponding upper bound on the H^+ densities in the center of the torus is ~ 5 cm^{-3}. If we assume that the relatively large ion thermal speeds corresponding to ion temperatures as high as 5 X 10^6 °K do not severely violate the conditions for Jordon's [1969] calculations of ionization equilibrium for oxygen, the dominant charge state can be used to obtain a gross estimate of electron temperature at the orbits of Tethys and Dione, ~ 4-8 X 10^4 °K. Similarly the dominance of O^{3+} at ~ 7 R_S yields an electron temperature of ~ 10^5 °K. These electron temperatures are also consistent with an upper bound on the magnitude of the spacecraft potential relative to the ambient medium of ~ 10 to 20 volts as indicated by the good fits of the observed ion velocity distributions at energies $\geq$ 100 eV to unperturbed isotropic Maxwellian distributions.

Our current interpretation of the presence of a large oxygen torus which engulfs the orbits of Dione and Tethys is that water is photodissociated or dissociated by charged particles as a source of atomic hydrogen H and the radical OH. These products then are ionized by either electron impact and/or photoionization. Overall the qualitative nature of the temperature and density profiles in Saturn's oxygen torus are similar to

those for the sulfur ion torus within Jupiter's magnetosphere at Io's orbit [cf. Bagenal et al., 1980]. In particular the steep temperature gradient extending from approximately Dione's orbit to 4.1 R_S is similar to that observed in the vicinity of Io. In the present case too, the temperature ratio of a factor of 10 for temperatures at 7 R_S relative to those at 4 R_S is much greater than that expected for simple corotational pickup of an ionized neutral. The corotational energies for oxygen ions at 4 R_S and 7.5 R_S are 135 eV and 470 eV, respectively. Bagenal et al. [1980] interpret the temperature gradient inside the orbit of Io as the inward diffusion and radiative cooling of sulfur ions. For Saturn's plasma torus, a similar interpretation invokes the diffusion and radiative cooling of oxygen ions inward from the orbit of Dione. We can roughly estimate the order of magnitude of the diffusive loss of plasma via the relationship for the diffusion flux $F = -D\ \Delta N/\Delta R$ where D is the diffusion coefficient, and $\Delta N/\Delta R$ is the density gradient. We take $\Delta N \sim 50$ cm^{-3} and $\Delta R \sim 3$ R_S from our present observations and assume that $D \sim 10^{-9}$ to 10^{-10} R_S^2/sec. This latter assumption for the value of D is based upon values $\sim 10^{-10}$ R_S^2/sec for protons with energies > 80 MeV in Saturn's magnetosphere [Van Allen et al., 1980b], and is used here in lieu of a more satisfactory means of estimating D [cf. Siscoe, 1978]. The order of magnitude of the diffusion flux F becomes 3×10^1 to 3×10^2 ions/cm^2-sec. If we assume that the thickness of the torus is 4 R_S then the total ion flux inwards from the torus toward Saturn is $\sim 1.5 \times 10^{23}$ to 1.5×10^{24} ions/sec. From this crude estimate for diffusive loss we can estimate the source strength at the surface of Dione. Carlson [1980] has considered various mechanisms for the dissociation of water on ice surfaces of

the ring material, including photo-sputtering [Harrison and Schoen, 1967], magnetospheric ion sputtering [Cheng and Lanzerotti, 1978] and sublimation with subsequent photodissociation [Blamont, 1974], and concluded that photo-sputtering provides the largest source rate. The corresponding flux escaping from the water frost is ~ 10^8 H atoms/cm^2-sec for a molecular photodissociation rate of 1.1 X 10^{-7}/molecule-sec. If we assume that (1) a similar mechanism is operative on Dione, (2) the OH flux is equal to that for atomic hydrogen and (3) the diffusive loss rate estimated above is the dominant loss rate for the plasma torus, then the flux of OH radicals at Dione's surface must be ~ 2 X 10^7 to 2 X 10^8/cm^2-sec and consistent with the capabilities of the photo-sputtering. Since Tethys is characterized with a similar mass and radius as those for Dione [cf. Cruikshank, 1978] and is also believed to be ice-covered, this satellite would be expected to provide a source of oxygen ions of similar magnitude. It is noted here that if our estimates of electron thermal energies, ~ 5 to 10 eV, as inferred from the oxygen charge states are correct, then the surfaces of both satellites Dione and Tethys are exposed to an electron flux ~ 10^{10}/cm^2-sec with these energies and could produce a significant contribution to the molecular dissociation rates via electron impact. The binding energy for H-OH is 5.16 eV [Dennefeld, 1974]. The radial extent of the plasma torus is consistent with the photodissociation of water. If, for example, a mechanical energy of 3 eV is available after photodissociation and excitation of the vibrational and electronic states of OH, these radicals can be injected into elliptical orbits spanning the radial distance range of ~ 5.5 to 7.3 R_s. Atomic hydrogen acquires escape

velocity, a fact that can account for the general relative absence of protons in the plasma torus. On the other hand, in the simplest model, the ion temperature due to corotational pickup of O^+ upon ionization of the OH radical is expected to be proportional to R^2 as contrasted to the observed R^6 variation for $R \lesssim 7\ R_S$.

The principal reasons for considering Dione and Tethys as primary sources for the oxygen torus surrounding Saturn are (1) the very suggestive peaks in ion densities at their orbits (cf. Figure 8), (2) their surfaces are known to be covered with water ice or frost and thus an apparent source of oxygen via dissociation and ionization and (3) the ion density and temperature radial profiles are qualitatively similar to those for sulfur ions at the orbit of Io in Jupiter's magnetosphere. On the other hand, the temperature profile in the vicinity of the orbits of these two satellites shows no clear signature of their presence. Since Rhea is also covered with water frost [cf. Cruikshank, 1978] and its mass and radius are only factors of 2.1 and 1.6, respectively, greater than those of Dione [Anderson, 1980], substantial ion densities are also expected if the principal source is photo-sputtering of water on the satellite surfaces. No such signature in the ion densities is found at Rhea's orbit. Sublimation, a source of lesser magnitude, is appreciably affected by the radius and mass of the body. It is quite possible, in view of the findings of substantial atomic hydrogen densities in the vicinity of the rings [Judge *et al.*, 1980], that Dione and Tethys are only minor contributors to the overall oxygen population of the plasma torus. Earth-based measurements of the resonantly-scattered Lyman-α emissions of this hydrogen cloud are reported by Weiser *et al.* [1977].

In this interpretation the rapid density gradient at 4 R_S in the vicinity of the orbit of Enceladus is due to a combination of decreasing ion temperatures and corotation speeds to the extent that the ion energies are below the energy threshold, E/Q = 100 eV, of the plasma instrument. This possibility is strikingly suggested in the character of the spectrograms of Plate 1 for ~ 1400 ERT. The outer edge of the A ring is positioned only about 1.5 R_S away from the termination of usable responses of the plasma instrument at 4.1 R_S. The source rate necessary to support the atomic hydrogen densities in the vicinity of the rings is ~ 3 X 10^{28} atoms/sec, and is consistent with the mechanism of photo-sputtering of ring ice material [Carlson, 1980]. This source rate is a factor of ~ 3 X 10^4 greater than that from photo-sputtering from the surface of Dione or Tethys. The actual number of oxygen ions from ionization of OH and escaping impact with ring material is difficult to estimate without further calculations. In this interpretation the ions diffuse outward from the rings, are rapidly heated as a function of increasing radial distance and subsequently gain sufficient thermal and corotational energies to be observed with the plasma instrument at ~ 4 R_S. Thus heating of the oxygen ions is required as the ions diffuse radially outward to ~ 6.5 R_S where a high-β plasma occurs.

In summary, due to (1) the monotonically increasing temperatures with increasing radial distance in the torus, which are unaffected by the presence of Dione and Tethys and (2) the substantially greater potential source rate for OH radicals at the rings, we favor the rings as the primary source of torus plasmas and suggest Dione and Tethys as secondary

sources as evidenced by increases of oxygen ion densities at their orbits. This interpretation will also yield the substantially lesser oxygen ion temperatures that are observed relative to those expected for corotational pickup since, at the outer edge of the A ring at 2.3 R_S, the neutral particle orbital speed differs from the corotation speed by only ~ 7 km/sec which corresponds to an oxygen ion temperature of ~ 5 X 10^4 °K. These observations indicate the possibility of a torus of H_2O and OH in the vicinity of the orbits of Dione and Tethys with substantially lesser densities than those at the rings. The diffuse hot component of the oxygen velocity distributions detected with the plasma instrument in the torus (cf. Figure 7) could be the signature of the ionization of OH from Dione and Tethys. For example the oxygen temperature corresponding to corotational pickup with ionization of OH is ~ 3 X 10^6 °K. The observed temperature, if the ions in the high-speed tail of the velocity distribution are O^{2+}, is ~ 5 X 10^6 °K.

The source of the protons observed at radial distances beyond 8.8 R_S is not clearly resolved here. One possibility is that these protons are the ionization products of a tenuous gas of atomic hydrogen from the dissociation of water frost on the ring material. Photo-sputtering will allow atomic hydrogen to gain escape velocity and thus provide a source mechanism at these radial distances. The substantially fluctuating ion temperatures and densities at $R > 8.8\ R_S$ suggest rapid temporal variations in the topology of the outer magnetosphere. Other possible sources for these low-energy protons include the magnetosheath, Titan (the dayside magnetopause was crossed inside Titan's orbit during a period of enhanced solar wind pressure), and Saturn's ionosphere. With the current

measurements, it does not appear possible to clearly distinguish among these four sources for ions in the outer magnetosphere.

In the spirit of speculation, it is noted here that if the plasma torus extends inward to the rings of Saturn the satellite Enceladus will be nonuniformly exposed to a large flux of oxygen ions on its trailing face since the corotational bulk flow speed exceeds the satellite orbital speed by 28 km/sec. There is evidence that the trailing face of Enceladus is brighter due to the presence of water frost than the leading face [Cruikshank, 1978]. The oxygen flux is estimated here at $\sim 1.5 \times 10^8$ ions/cm^2-sec. For comparison the photo-sputtering loss rates are $\sim 1 \times 10^8$ molecules/cm^2-sec and the sublimation rate for water frost at 100°K is $\sim 5 \times 10^5$ molecules/cm^2-sec [Dennefeld, 1974]. It is possible that the recombination of the oxygen and hydrogen produces water frost preferentially on the trailing face.

A constant source of oxygen ions and their subsequent energization in the plasma torus, and the observational fact that the β of the plasma torus is of the order of unity as deep in Saturn's magnetosphere as 6.5 R_S, suggest that the plasma pressure may be periodically relieved by spontaneous plasma outflow through the magnetotail. We note here that the condition for plasma outflow in a rotating dipole field [Hill *et al.*, 1974] is approximately met over the radial distance range 6 to 8 R_S. This condition requires that the corotational energy density of the plasma is equal to or greater than the energy density of the dipole magnetic field. Major reconfigurations of the magnetosphere beyond these radial distances can also be expected. The total number of oxygen ions in the

torus, assuming a thickness of 4 R_S is ~ 2 X 10^{33} ions. If the source of ions is photo-sputtering from the surface of Dione and in the unlikely situation that there are no significant losses, the torus-filling time is ~ (2 X 10^{33} ions)/(7 X 10^{23} ions/sec) ≈ 3 X 10^9 seconds (100 years). On the other hand, if the oxygen source rate is only 1% of the source rate for atomic hydrogen at the rings as estimated by Carlson [1980], then this torus-filling time is ~ (2 X 10^{33} ions)/(3 X 10^{26} ions/sec) ≈ 7 X 10^6 seconds (81 days). The corresponding diffusion coefficient D is ~ 5 X 10^{-7} R_S^2/sec and the average radial drift speed is ~ 10^{-2} km/sec. If the absence of density minima at the satellite orbits is interpreted in terms of drift speeds sufficiently great to provide displacements comparable to or greater than the diameter of Dione or Tethys in one plasma corotational period, the corresponding lower limit on the drift speed is ~ (1000 km)/(3.7 X 10^4 sec) ≈ 3 X 10^{-2} km/sec. Thus a ring source for the oxygen ions can profoundly affect magnetospheric configuration and dynamics beyond ~ 6 R_S. The next series of <u>in situ</u> measurements will be gained with the Voyager spacecraft. The above calculations indicate that the torus configuration could be greatly different relative to that reported above for the Pioneer 11 encounter.

Appendix: Plasma Analyzer Responses to a Corotating Maxwellian Velocity Distribution

We summarize here our treatment of the responses of the high-resolution electrostatic analyzer to a corotating plasma within Saturn's magnetosphere. For the measurements presented herein the center of the field-of-view of sensor 1 is directed at 50.4° to the spacecraft spin axis. The responses of this sensor are accumulated onboard only for each of two one-half spin periods (see Figure 1). The average directional, differential intensity of positive ions for a half spin period, $dJ/dEd\Omega$, is related to the corresponding accumulated counts, C,

$$\frac{dJ}{dEd\Omega} = \frac{4.64X10^4C}{MV^2} , \tag{1}$$

where M and V are the ion mass and velocity, respectively. Cgs units are employed throughout the discussion. The average phase space density, $\overline{n(V)}$ in units of sec^3/cm^6, is related to above intensities,

$$\overline{n(V)} = \frac{M}{V^2}\frac{dJ}{dEd\Omega} , \tag{2}$$

thus yielding

$$\overline{n(V)} = \frac{4.64X10^4C}{V^4} . \tag{3}$$

For a given V, or E/Q, two determinations of the average n(V) are observed with the plasma analyzer, one each for the two half-spin accumulation periods.

We must now find the expected responses of the instrument to a corotating Maxwellian plasma with number density N, temperature T and corotating velocity vector $\vec{V}_o$ in the spacecraft reference frame. This corotation speed is sufficiently large to allow neglect of the spacecraft velocity vector relative to Saturn in the present approximation. For the corotating Maxwellian

$$n(V) = \frac{N}{\left(\frac{2\pi kT}{M}\right)^{3/2}} \exp(-MV'^2/2kT) , \tag{4}$$

where $\vec{V}' = \vec{V}-\vec{V}_o$. Note that for a given value of n(V), the temperature T is proportional to mass M. Hence two ions with the same M/Q value, for example H_2^+ and He^{2+}, will have identical velocity distributions if $T(He^{2+}) = 2T(H_2^+)$. Thus the ion must be identified for an accurate assessment of the temperature T. Since the electrostatic analyzer is capable of assessing only M/Q, determination of the plasma temperature T depends critically on the mass of the assumed ion. The average densities $\overline{n(V)}$ for the two half-spins are

$$\overline{n(V)} = \frac{1}{\pi}\int_{\phi'}^{\phi'+\pi} n(V)d\phi \tag{5}$$

with $\phi' = \pi/2$ and $3\pi/2$, respectively. The angle ϕ is the spin phase angle for the spacecraft rotation and is referenced to $\phi = 0°$ when the sensor field-of-view is parallel to the ecliptic and ascending toward the north ecliptic pole.

In order to numerically integrate equation (5), $\vec{V}_o \cdot \vec{V}$ must be determined as a function of spin phase angle ϕ. The ecliptic-equinox coordinate system (epoch 1950.0) can be conveniently utilized to evaluate $\vec{V}_o \cdot \vec{V}$. The X^e-axis is directed toward the vernal equinox and the Z^e-axis toward the north ecliptic pole. The positive-ion velocity vectors $\vec{V}^e$ viewed by the sensor as a function of ϕ in these coordinates are

$$\vec{V}^e = \begin{bmatrix} -V \cos\theta_o \cos\beta \cos\alpha - V \sin\theta_o \cos\phi \sin\beta + V \sin\theta_o \sin\phi \cos\beta \sin\alpha \\ V \cos\theta_o \sin\beta \cos\alpha - V \sin\theta_o \cos\phi \cos\beta - V \sin\theta_o \sin\phi \sin\beta \sin\alpha \\ -V \cos\theta_o \sin\alpha_o - V \sin\theta_o \sin\phi \cos\alpha \end{bmatrix} \qquad (6)$$

with $\theta_o = 50.4°$ and spacecraft spin axis direction $\alpha = -1.8°$, $\beta = 14.7°$. In order to find the corotational velocity vector $\vec{V}_o$ in the ecliptic-equinox coordinates it is necessary to first find the spacecraft position in Saturn spin-axis coordinates, $\vec{X}^s_{sc}$, then to determine $\vec{V}^s_o$ in these coordinates and subsequently transform this vector into ecliptic-equinox coordinates, $\vec{V}^e_o$. The spacecraft position is

$$\vec{X}^s_{sc} = \begin{bmatrix} \cos\theta^e \cos\phi^e X^e_{sc} + \cos\theta^e \sin\phi^e Y^e_{sc} - \sin\theta^e Z^e_{sc} \\ -\sin\phi^e X^e_{sc} + \cos\phi^e Y^e_{sc} \\ \sin\theta^e \cos\phi^e X^e_{sc} + \sin\theta^e \sin\phi^e Y^e_{sc} + \cos\theta^e Z^e_{sc} \end{bmatrix} \qquad (7)$$

where $\theta^e = 28.1°$, $\phi^e = 78.8°$ is the direction of the Saturn spin axis and $\vec{X}^e_{sc}$ is the spacecraft position in Saturn-centered ecliptic-equinox coordinates. The corotational velocity in ecliptic-equinox coordinates becomes

$$\vec{V}^e_o = \begin{bmatrix} -\omega R \cos\theta^s_{sc} \sin\phi^s_{sc} \cos\phi^{ss} \cos\theta^{ss} + \omega R \cos\theta^s_{sc} \cos\phi^s_{sc} \sin\phi^{ss} \\ \omega R \cos\theta^s_{sc} \sin\phi^s_{sc} \sin\phi^{ss} \cos\theta^{ss} + \omega R \cos\theta^s_{sc} \cos\phi^s_{sc} \cos\phi^{ss} \\ -\omega R \cos\theta^s_{sc} \sin\phi^s_{sc} \sin\theta^{ss} \end{bmatrix} \qquad (8)$$

where the Saturn angular rotation speed $\omega = 1.73 \times 10^{-4}$ rad/sec, R is the radial distance from Saturn to the spacecraft, $\theta^s_{sc} = \text{Arcsin}\,(Z^s_{sc}/R)$, $\phi^s_{sc} = \text{Arctan}\,(Y^s_{sc}/X^s_{sc})$ and the Saturn spin axis direction $\theta^{ss} = -28.1°$, $\phi^{ss} = -78.8°$.

The above transformations (6) and (8) allow numerical integration of the two integrals (5) which are directly related to the observed average densities (3). Increments of $\Delta\phi = 1.2 \times 10^{-2}$ radian are chosen for the numerical integration. A nonlinear least square fit which utilizes the method proposed by Gauss (courtesy of K. Sando, Chemistry Department) [cf. McWilliams et al., 1965] is employed to determine N and T from the integral (5) corresponding to the angular sector closest to the direction of corotation, $\phi' = \pi/2$, for a given ion mass M. This best-fit computation for N and T is repeated for M = 1, 2, 4, 8 and 16 amu. The plasma analyzer is not capable of direct identification of the ion species. However, the information concerning angular distributions available from the two integrals (5), $\phi' = \pi/2$ and $\phi' = 3\pi/2$, with the above assumption of a corotating Maxwellian distribution, allows an indirect determination of the

mass-per-unit charge (M/Q) values for the positive ions. Hence the observed $\overline{n(V)}$, (3) above, in the spin sector generally directed away from the corotation can be used for comparison with the computed $\overline{n(V)}$ for $\phi' = 3\pi/2$ to find an approximate value for M/Q by imposing the best-fit N and T from (5) for $\phi' = \pi/2$. The counting statistics for measurements corresponding to the integral $\phi' = 3\pi/2$ are not always sufficient for such species identification (cf. Figure 6). These extensive numerical computations are performed for each of the 62 individual measurements of ion velocity distributions within Saturn's dayside magnetosphere as presented in the text.

Acknowledgments

The authors appreciate the concise summary of spacecraft trajectory and attitude parameters that was supplied by J. A. Van Allen. This research was supported in part by the National Aeronautics and Space Administration under grant NGL-16-001-002.

References

Anderson, J. D., G. W. Null, E. D. Biller, S. K. Wong, W. B. Hubbard and J. J. MacFarlane, Pioneer Saturn celestial mechanics experiment, Science, 207, 449, 1980.

Bagenal, F., J. D. Sullivan and G. L. Siscoe, Spatial distribution of plasma in the Io torus, Geophys. Res. Lett., 7, 41, 1980.

Blamont, J., The "atmosphere" of the rings of Saturn, in The Rings of Saturn, ed. by F. D. Palluconi and G. H. Pettengill, NASA SP-343, p. 125, 1974.

Carlson, R. W., Photo-sputtering of ice and hydrogen around Saturn's rings, Nature, 283, 461, 1980.

Cheng, A. F. and L. J. Lanzerotti, Ice sputtering by radiation belt protons and the rings of Saturn and Uranus, J. Geophys. Res., 83, 2597, 1978.

Cruikshank, D. P., Physical properties of the satellites of Saturn, in The Saturn System, ed. by D. M. Hunten and D. Morrison, NASA Conference Publication 2068, p. 217, 1978.

Dennefeld, M., Theoretical studies of an atmosphere around Saturn's rings, in Exploration of the Planetary System, ed. by A. Woszczyk and C. Iwaniszewska, D. Reidel Publishing Company, p. 471, 1974.

Fillius, W., W. H. Ip and C. E. McIlwain, Trapped radiation belts of Saturn: First look, Science, 207, 425, 1980.

Fink, U., H. P. Larson, T. N. Gautier III and R. R. Treffers, Infra-red spectra of the satellites of Saturn: Identification of water ice on Iapetus, Rhea, Dione, and Tethys, Astrophys. J., 207, L63, 1976.

Gurnett, D. A., L. A. Frank and R. P. Lepping, Plasma waves in the distant magnetotail, J. Geophys. Res., 81, 6059, 1976.

Harrison, H. and R. I. Schoen, Evaporation of ice in space: Saturn's rings, Science, 157, 1175, 1967.

Hill, T. W., A. J. Dessler and F. C. Michel, Configuration of the Jovian magnetosphere, Geophys. Res. Lett., 1, 3, 1974.

Jordan, C., The ionization equilibrium of elements between carbon and nickel, Mon. Not. R. Astr. Soc., 142, 501, 1969.

Judge, D. L., F.-M. Wu and R. W. Carlson, Ultraviolet photometer observations of the Saturnian system, Science, 207, 431, 1980.

Kuiper, G. P., D. P. Cruikshank and U. Fink, The composition of Saturn's rings, Sky and Tel., 39, 14, 1970.

McWilliams, P., W. S. Hall and H. E. Wegner, Multichannel analyzer data analysis by a least squares computer program, Rev. Sci. Instr., 33, 70, 1965.

Morrison, D., D. P. Cruikshank, C. B. Pilcher and G. H. Rieke, Surface compositions of the satellites of Saturn from infrared photometry, Astrophys. J., 207, L213, 1976.

Pilcher, C. B., C. R. Chapman, L. A. Lebovsky and H. H. Kieffer, Saturn's rings: Identification of water frost, Science, 167, 1372, 1970.

Simpson, J. A., T. S. Bastian, D. L. Chenette, G. A. Lentz, R. B. McKibben, K. R. Pyle and A. J. Tuzzolino, Saturnian trapped radiation and its absorption by satellites and rings: The first results from Pioneer 11, Science, 207, 411, 1980.

Siscoe, G. L., Magnetosphere of Saturn, in The Saturn System, ed. by D. M. Hunten and D. Morrison, NASA Conference Publication 2068, p. 265, 1978.

Smith, E. J., L. Davis, Jr., D. E. Jones, P. J. Coleman, Jr., D. S. Colburn, P. Dyal and C. P. Sonett, Saturn's magnetic field and magnetosphere, Science, 207, 407, 1980.

Trainor, J. H., F. B. McDonald and A. W. Schardt, Observations of energetic ions and electrons in Saturn's magnetosphere, Science, 207, 421, 1980.

Van Allen, J. A., M. F. Thomsen, B. A. Randall, R. L. Rairden and C. L. Grosskreutz, Saturn's magnetosphere, rings and inner satellites, Science, 207, 415, 1980a.

Van Allen, J. A., B. A. Randall and M. F. Thomsen, Sources and sinks of energetic electrons and protons in Saturn's magnetosphere, J. Geophys. Res., 85, (this issue), 1980b.

Weiser, H., R. C. Vitz and H. W. Moos, Detection of Lyman-α emission from the Saturnian disk and from the ring system, Science, 197, 755, 1977.

Wolfe, J. H., J. D. Mihalov, H. R. Collard, D. D. McKibbin, L. A. Frank and D. S. Intriligator, Pioneer 10 observations of the solar wind interaction with Jupiter, J. Geophys. Res., 79, 3489, 1974.

Wolfe, J. H., J. D. Mihalov, H. R. Collard, D. D. McKibbin, L. A. Frank and D. S. Intriligator, Preliminary results on the plasma environment of Saturn from the Pioneer 11 plasma analyzer experiment, Science, 207, 403, 1980.

Plate Caption

Plate 1. Color-coded energy-time spectrograms for the responses of the high-resolution plasma analyzer on board Pioneer 11 to low-energy positive ions as this spacecraft traverses the dayside magnetosphere of Saturn during 0000 to 1650 ERT (UT of receipt of signal at earth) on September 1, 1979. (See text for details of spectrograms.) The upper spectrogram summarizes responses during which the field-of-view for sensor 1 of the plasma analyzer is generally directed toward the corotational flow, and the bottom spectrogram displays responses when the field-of-view is scanning directions at larger angles to the corotational flow vector. A large torus of oxygen ions is encountered during the period ~ 1000 to 1500 ERT. The high responses at ~ 1500 to 1630 ERT are due to penetrating energetic charged particles. The responses in the upper spectrogram are identified in the present analysis as those corresponding to angular sector $\phi' = \pi/2$, and those of the bottom spectrogram to angular sector $\phi' = 3\pi/2$.

Note: This plate is to be published in color.

Figure Captions

Figure 1. The left-hand panel shows the trajectory of Pioneer 11 as projected onto Saturn's equatorial plane during the period of plasma measurements displayed in Plate 1. Angular sampling of the plasma velocity distributions with sensor 1 of the plasma analyzer is summarized with the right-hand diagrams. The axis of the sensor's field-of-view is directed at an angle 50.4° to the spacecraft spin axis. The responses of the sensor are accumulated for two angular sectors each corresponding to one-half spin period of the spacecraft and referenced to the ascending crossing of the ecliptic plane. These two angular sectors are referred to herein as $\phi' = \pi/2$ and $\phi' = 3\pi/2$, respectively.

Figure 2. Best nonlinear least-squares fits of corotating hydrogen velocity distributions with various fractions of the rigid corotation speed V_o to the observed ion velocity distributions in the outer magnetosphere at 15.7 R_s (1 R_s = Saturn radius = 6 X 10^4 km). The corotation speed V_o is 160 km/sec. A good fit is obtained for a speed of 0.5 V_o, or 80 km/sec.

Figure 3. Continuation of Figure 2 for the ion velocity distribution observed at 0117 ERT (15.1 R_s). A good fit to a corotating Maxwellian is not found for this series of observations.

Figure 4. Best nonlinear least-squares fits for the ion velocity distributions observed at 7.1 R_S in the plasma torus, assuming values of M/Q = 1(H^+), 4(He^+), 8(O^{2+}) and 16(O^+). The overall best fit is for a species with M/Q between 4 and 8.

Figure 5. Continuation of Figure 4 for ion velocity distributions observed at 1219 ERT (6.4 R_S). The best overall fit is for O^{2+} with a density N = 40.8 cm^{-3} and a temperature T = 1.6 X 10^6 °K. The corotation speed is 65 km/sec.

Figure 6. Continuation of Figure 4 for five representative ion species at 5.6 R_S where the ion temperature is sufficiently low that no usable responses are available f· · angular sector $\phi' = 3\pi/2$ which views large angles relative to the corotation bulk flow.

Figure 7. Best fits for the high-speed tails of the ion velocity distribution at 6.6 R_S. These ions are most likely O^{2+} or O^{3+} corresponding to the range of best-fit M values of ~ 4 to 8 amu. A substantial contribution to this ion velocity distribution by H^+ or O^+ ions appears to be excluded.

Figure 8. Ion densities, temperatures and dominant species as functions of planetocentric radial distance. Identification of the dominant ion species is discussed in detail in the text. The oxygen torus extends from ~ 4 R_S to 8 R_S. The rapid decline of densities at ~ 4 R_S may be due to ion energies decreasing with decreasing radial distance to values below the energy (E/Q) threshold of the plasma instrument at 100 eV-per-unit charge. Ion temperatures within the plasma torus at ~ 4 R_S to 7 R_S monotonically decrease with decreasing radial distance. The outer edge of the A ring is located at 2.3 R_S.

Figure 9. The ion energy density, ϵ in units of ergs/cm^3, and the ratio of plasma and magnetic field pressures, β, as functions of radial distance. Note the relatively high values of β in the plasma torus as close to the planet as 6.4 R_S ($\beta \simeq 0.5$).

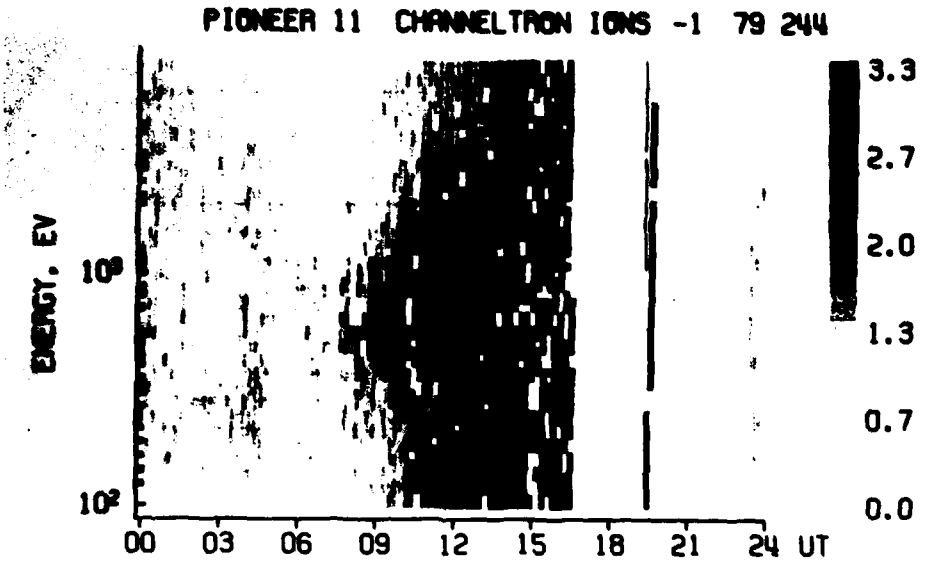
PIONEER 11 CHANNELTRON IONS -1 79 244
ENERGY, EV
10^3
10^2
00 03 06 09 12 15 18 21 24 UT
3.3
2.7
2.0
1.3
0.7
0.0

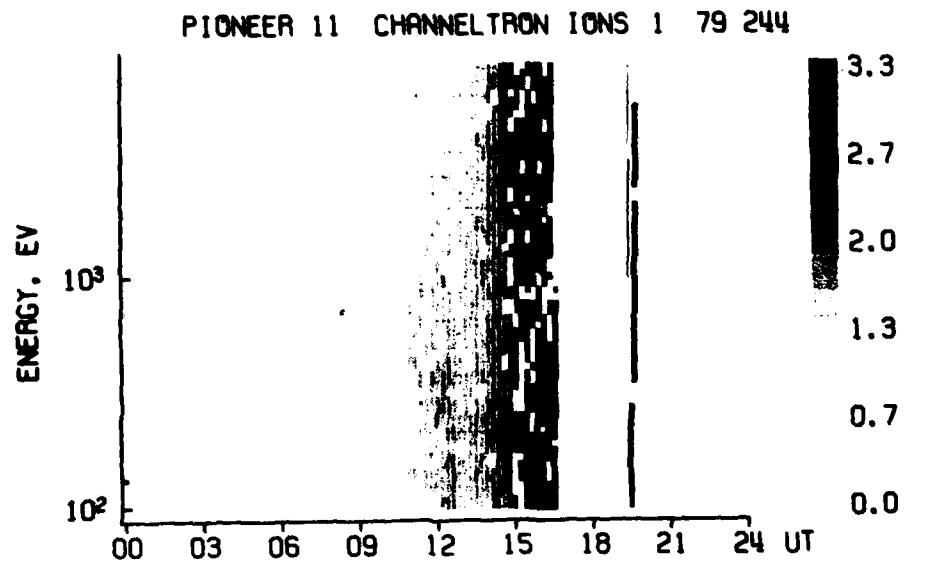
PIONEER 11 CHANNELTRON IONS 1 79 244
ENERGY, EV
10^3
10^2
00 03 06 09 12 15 18 21 24 UT
3.3
2.7
2.0
1.3
0.7
0.0

Plate 1

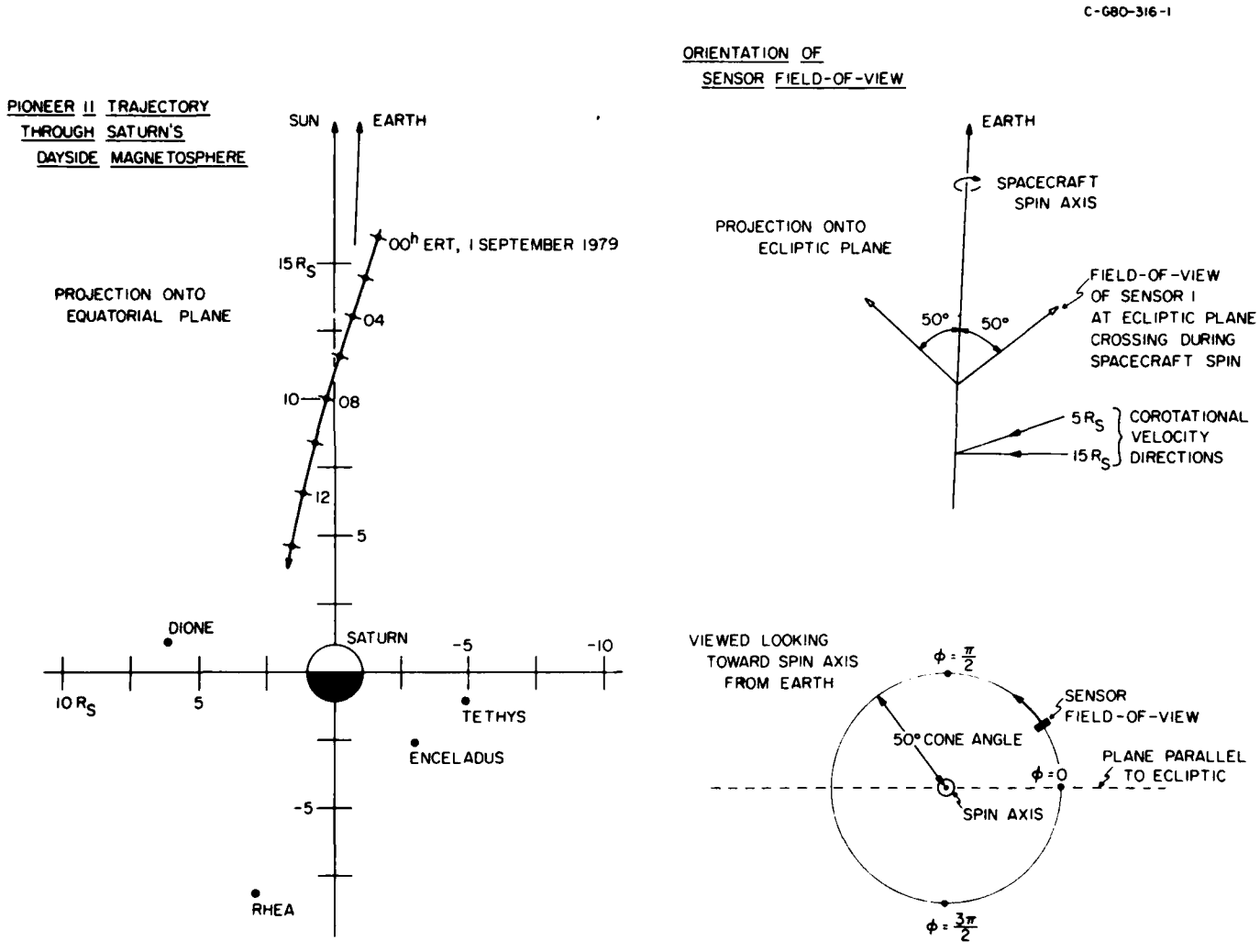
C-G80-316-1
PIONEER II TRAJECTORY THROUGH SATURN'S DAYSIDE MAGNETOSPHERE
PROJECTION ONTO EQUATORIAL PLANE
SUN
EARTH
00h ERT, 1 SEPTEMBER 1979
15 RS
04
10
08
12
5
DIONE
SATURN
-5
-10
10 RS
5
TETHYS
ENCELADUS
-5
RHEA
ORIENTATION OF SENSOR FIELD-OF-VIEW
PROJECTION ONTO ECLIPTIC PLANE
EARTH
SPACECRAFT SPIN AXIS
FIELD-OF-VIEW OF SENSOR 1 AT ECLIPTIC PLANE CROSSING DURING SPACECRAFT SPIN
50°
50°
5 RS
15 RS
COROTATIONAL VELOCITY DIRECTIONS
VIEWED LOOKING TOWARD SPIN AXIS FROM EARTH
ϕ = π/2
SENSOR FIELD-OF-VIEW
50° CONE ANGLE
ϕ = 0
PLANE PARALLEL TO ECLIPTIC
SPIN AXIS
ϕ = 3π/2

Figure 1

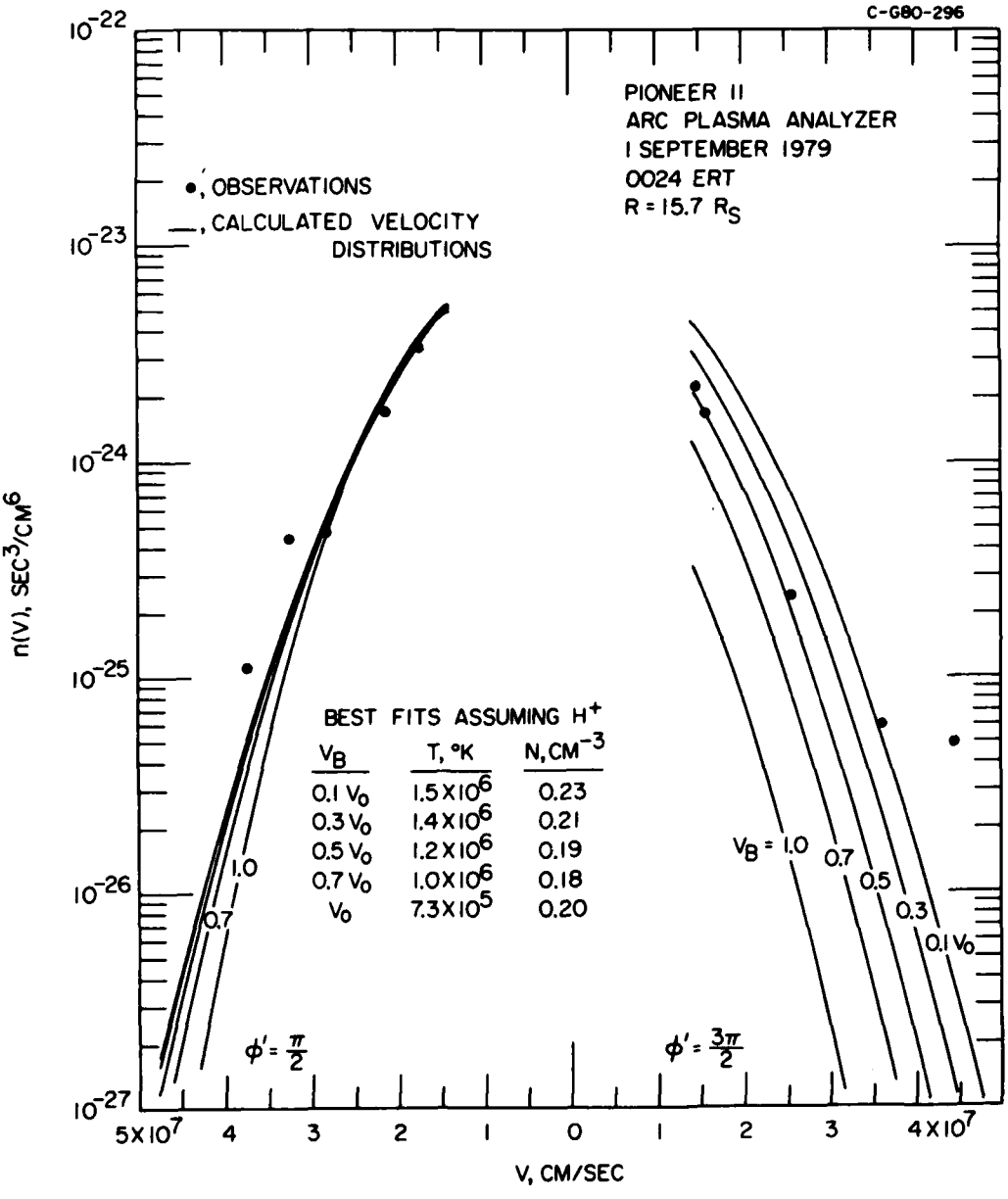
C-G80-296
PIONEER 11
ARC PLASMA ANALYZER
1 SEPTEMBER 1979
0024 ERT
R = 15.7 R_S
•, OBSERVATIONS
—, CALCULATED VELOCITY DISTRIBUTIONS
BEST FITS ASSUMING H^+
V_B | T, °K | N, CM^{-3}
0.1 V_0 | 1.5×10^6 | 0.23
0.3 V_0 | 1.4×10^6 | 0.21
0.5 V_0 | 1.2×10^6 | 0.19
0.7 V_0 | 1.0×10^6 | 0.18
V_0 | 7.3×10^5 | 0.20
V_B = 1.0
0.7
0.5
0.3
0.1 V_0
1.0
0.7
$\phi' = \frac{\pi}{2}$
$\phi' = \frac{3\pi}{2}$
10^{-22}
10^{-23}
10^{-24}
10^{-25}
10^{-26}
10^{-27}
n(V), SEC^3/CM^6
5×10^7 4 3 2 1 0 1 2 3 4×10^7
V, CM/SEC

Figure 2

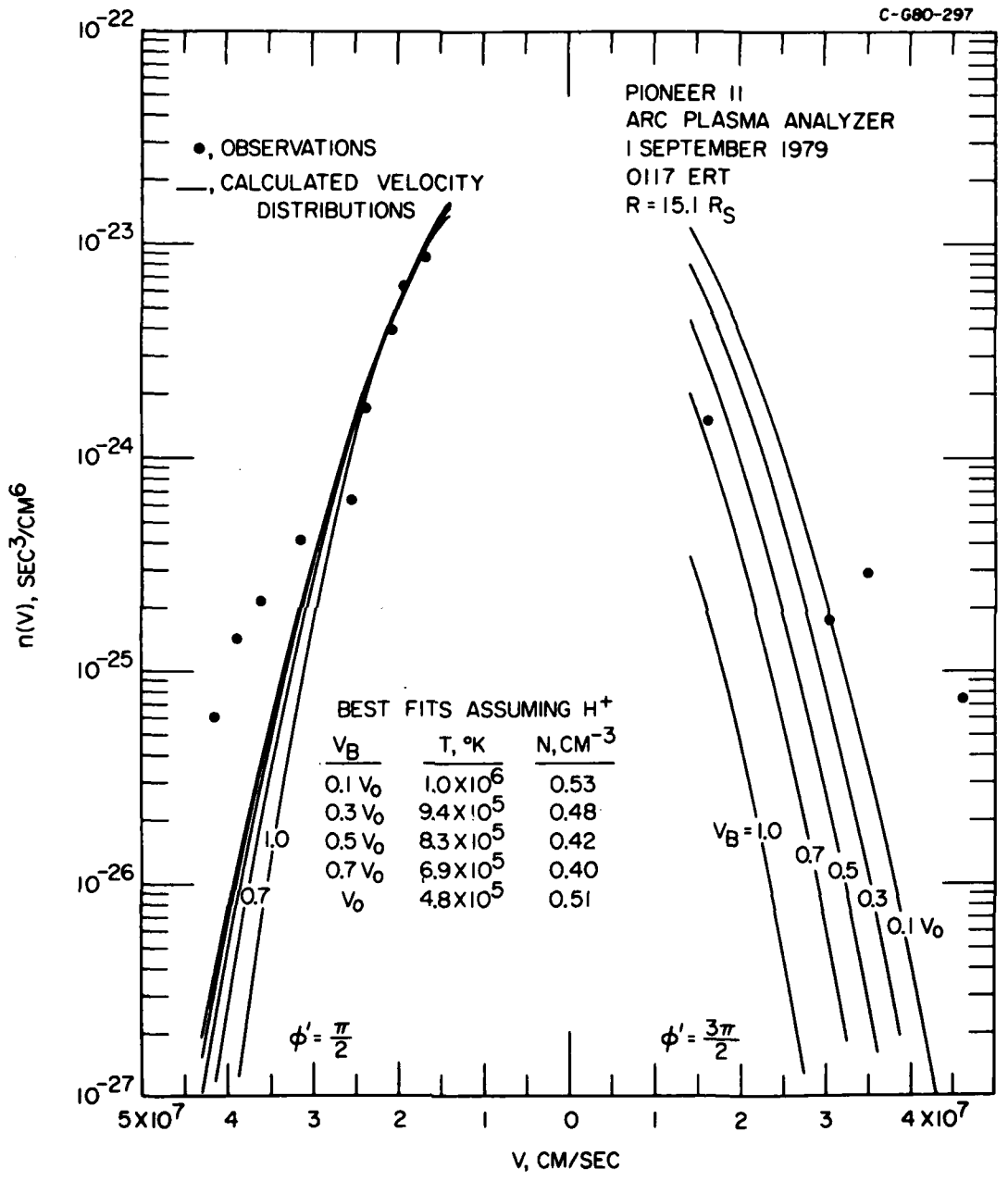
C-G80-297
PIONEER 11
ARC PLASMA ANALYZER
1 SEPTEMBER 1979
0117 ERT
R = 15.1 R_S
•, OBSERVATIONS
—, CALCULATED VELOCITY DISTRIBUTIONS
BEST FITS ASSUMING H+
V_B | T, °K | N, CM^-3
0.1 V_0 | 1.0X10^6 | 0.53
0.3 V_0 | 9.4X10^5 | 0.48
0.5 V_0 | 8.3X10^5 | 0.42
0.7 V_0 | 6.9X10^5 | 0.40
V_0 | 4.8X10^5 | 0.51
1.0
0.7
V_B = 1.0
0.7
0.5
0.3
0.1 V_0
φ' = π/2
φ' = 3π/2
n(V), SEC^3/CM^6
10^-22
10^-23
10^-24
10^-25
10^-26
10^-27
5X10^7
4
3
2
1
0
1
2
3
4X10^7
V, CM/SEC

Figure 3

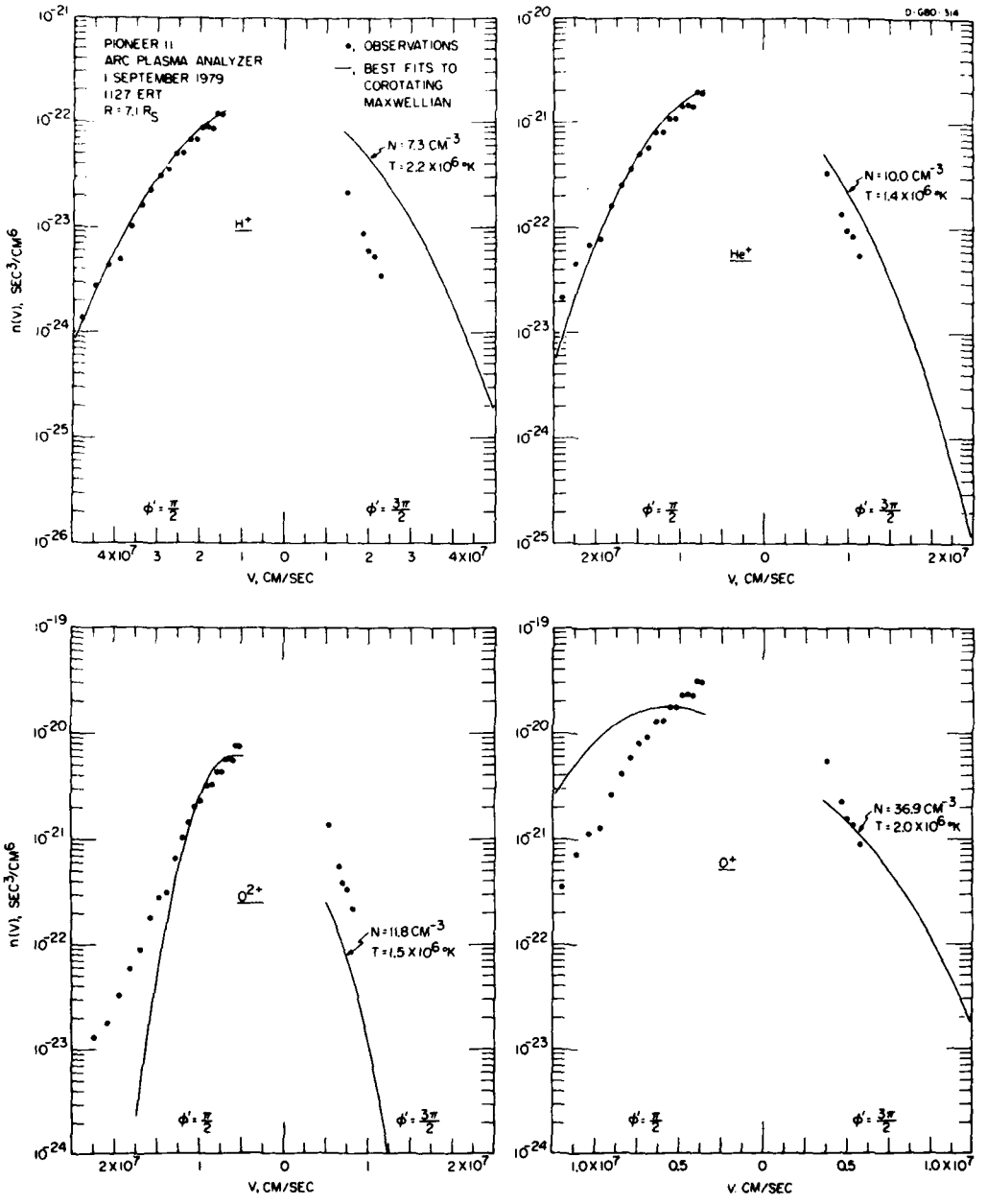
PIONEER 11
ARC PLASMA ANALYZER
1 SEPTEMBER 1979
1127 ERT
R = 7.1 R_S
•, OBSERVATIONS
—, BEST FITS TO COROTATING MAXWELLIAN
N = 7.3 CM^-3
T = 2.2 X 10^6 °K
H+
N = 10.0 CM^-3
T = 1.4 X 10^6 °K
He+
N = 11.8 CM^-3
T = 1.5 X 10^6 °K
O2+
N = 36.9 CM^-3
T = 2.0 X 10^6 °K
O+
n(V), SEC^3/CM^6
V, CM/SEC
φ' = π/2
φ' = 3π/2

Figure 4

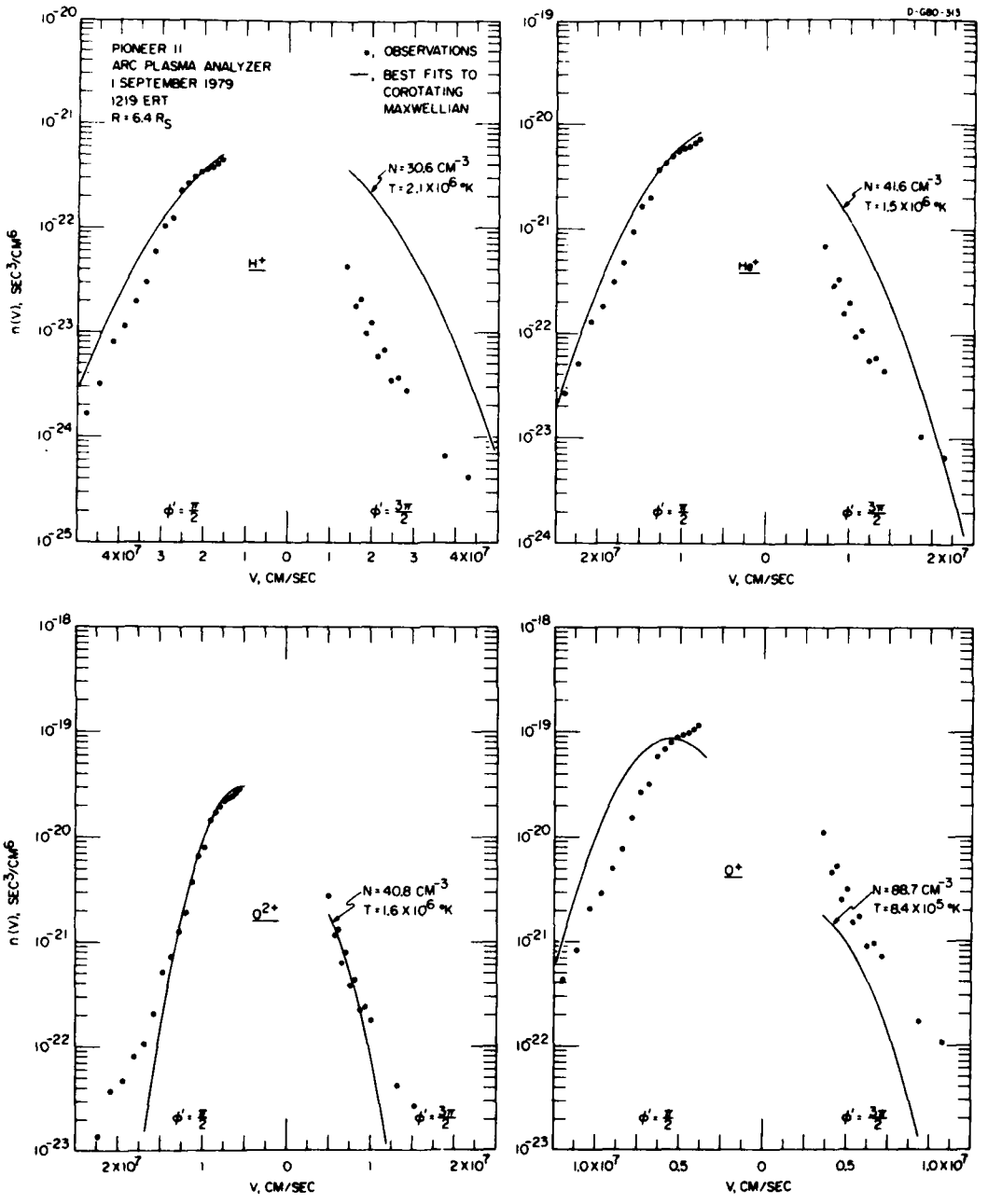
PIONEER 11
ARC PLASMA ANALYZER
1 SEPTEMBER 1979
1219 ERT
R = 6.4 R_S
•, OBSERVATIONS
—, BEST FITS TO COROTATING MAXWELLIAN
H+
N = 30.6 CM^-3
T = 2.1 X 10^6 °K
He+
N = 41.6 CM^-3
T = 1.5 X 10^6 °K
O2+
N = 40.8 CM^-3
T = 1.6 X 10^6 °K
O+
N = 88.7 CM^-3
T = 8.4 X 10^5 °K
n(V), SEC^3/CM^6
V, CM/SEC
D-GBO-343

Figure 5

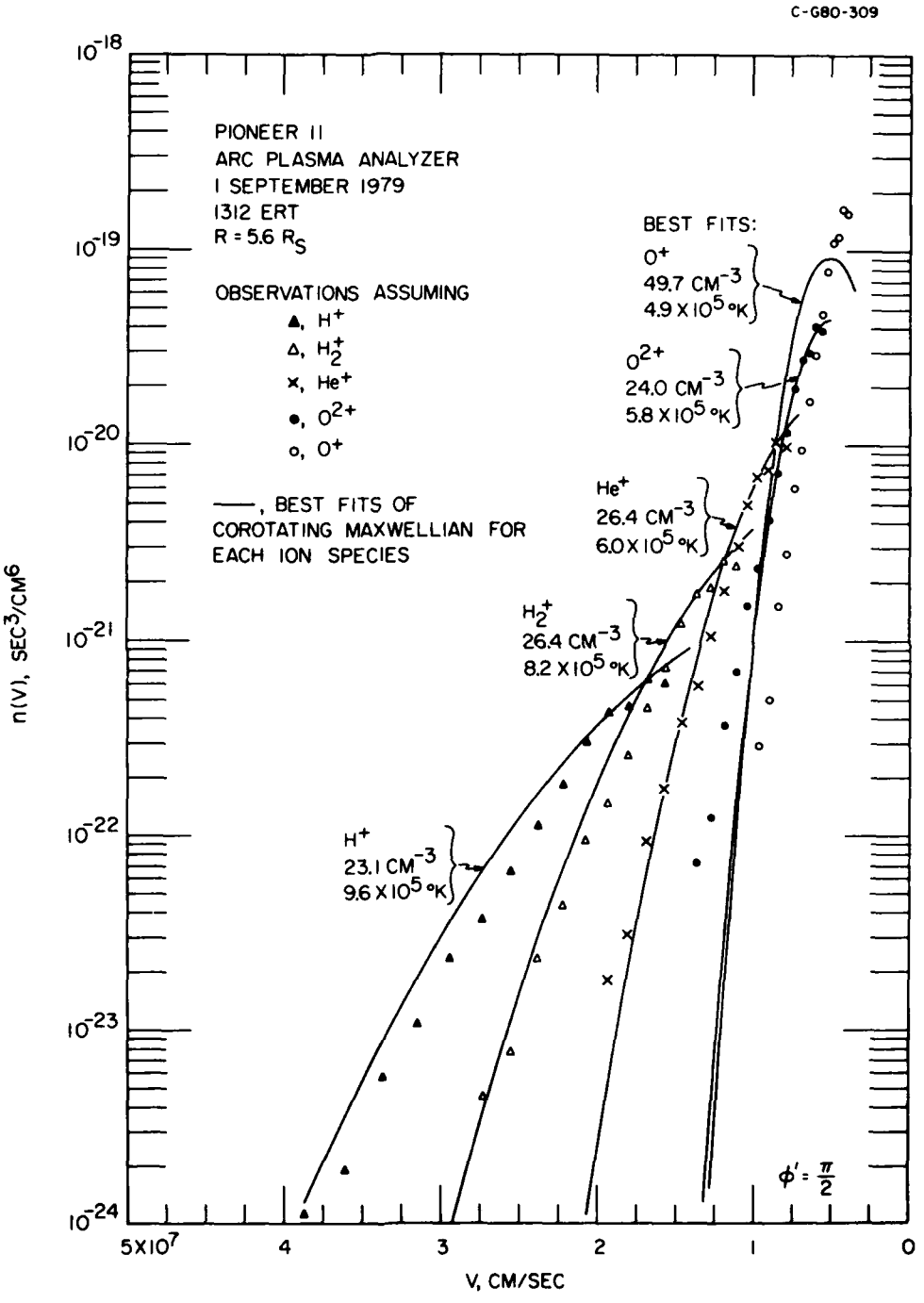
C-GBO-309
PIONEER 11
ARC PLASMA ANALYZER
1 SEPTEMBER 1979
1312 ERT
R = 5.6 R_S
OBSERVATIONS ASSUMING
▲, H^+
△, H_2^+
×, He^+
●, O^{2+}
○, O^+
——, BEST FITS OF COROTATING MAXWELLIAN FOR EACH ION SPECIES
BEST FITS:
O^+ 49.7 CM^{-3} 4.9 X 10^5 °K
O^{2+} 24.0 CM^{-3} 5.8 X 10^5 °K
He^+ 26.4 CM^{-3} 6.0 X 10^5 °K
H_2^+ 26.4 CM^{-3} 8.2 X 10^5 °K
H^+ 23.1 CM^{-3} 9.6 X 10^5 °K
$\phi' = \frac{\pi}{2}$
n(V), SEC^3/CM^6
10^{-18}
10^{-19}
10^{-20}
10^{-21}
10^{-22}
10^{-23}
10^{-24}
5X10^7
4
3
2
1
0
V, CM/SEC

Figure 6

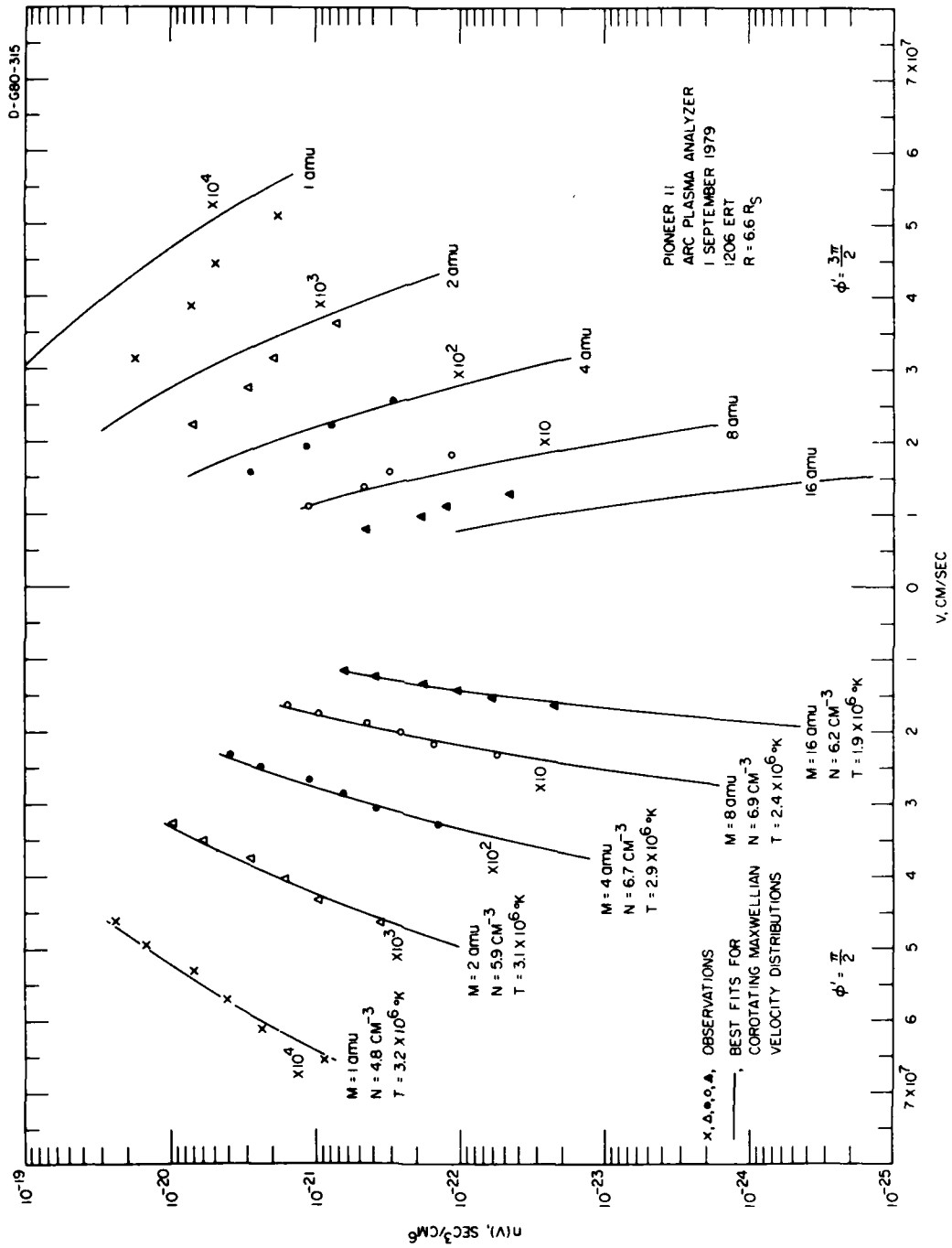
D-GBO-315
PIONEER II
ARC PLASMA ANALYZER
1 SEPTEMBER 1979
1206 ERT
R = 6.6 R_S
1 amu
2 amu
4 amu
8 amu
16 amu
x10⁴
x10³
x10²
x10
M = 1 amu
N = 4.8 CM⁻³
T = 3.2 x10⁶ °K
M = 2 amu
N = 5.9 CM⁻³
T = 3.1 x10⁶ °K
M = 4 amu
N = 6.7 CM⁻³
T = 2.9 x10⁶ °K
M = 8 amu
N = 6.9 CM⁻³
T = 2.4 x10⁶ °K
M = 16 amu
N = 6.2 CM⁻³
T = 1.9 x10⁶ °K
x, Δ, •, ○, ▲, OBSERVATIONS
——, BEST FITS FOR COROTATING MAXWELLIAN VELOCITY DISTRIBUTIONS
$\phi' = \frac{\pi}{2}$
$\phi' = \frac{3\pi}{2}$
n(V), SEC³/CM⁶
V, CM/SEC
10⁻¹⁹
10⁻²⁰
10⁻²¹
10⁻²²
10⁻²³
10⁻²⁴
10⁻²⁵
7x10⁷
6
5
4
3
2
1
0

Figure 7

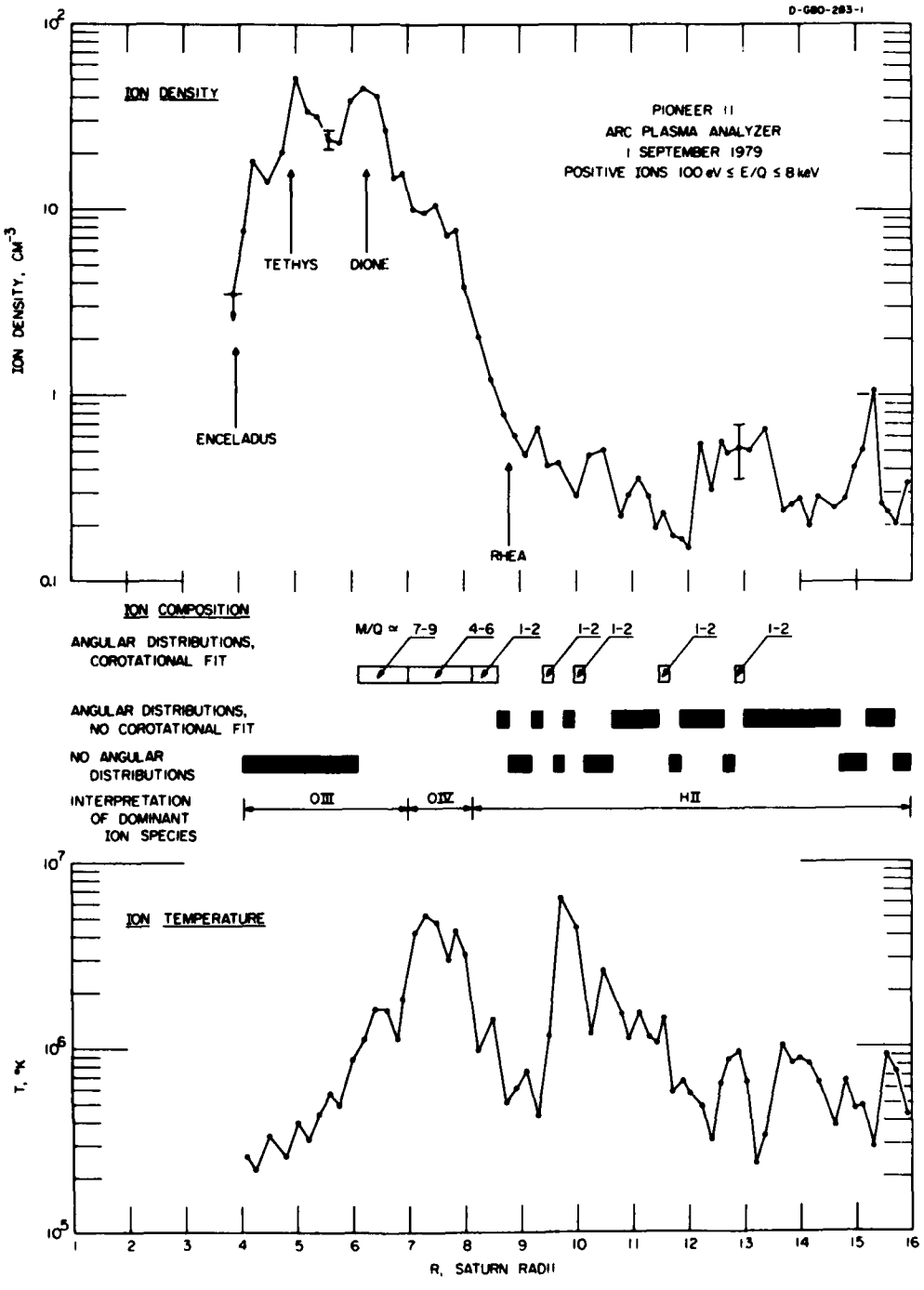
D-GBO-283-1
ION DENSITY
PIONEER 11
ARC PLASMA ANALYZER
1 SEPTEMBER 1979
POSITIVE IONS 100 eV ≤ E/Q ≤ 8 keV
ION DENSITY, CM⁻³
TETHYS
DIONE
ENCELADUS
RHEA
ION COMPOSITION
ANGULAR DISTRIBUTIONS, COROTATIONAL FIT
M/Q ≈ 7-9
4-6
1-2
1-2
1-2
1-2
1-2
ANGULAR DISTRIBUTIONS, NO COROTATIONAL FIT
NO ANGULAR DISTRIBUTIONS
INTERPRETATION OF DOMINANT ION SPECIES
OIII
OIV
HII
ION TEMPERATURE
T, °K
R, SATURN RADII

Figure 8

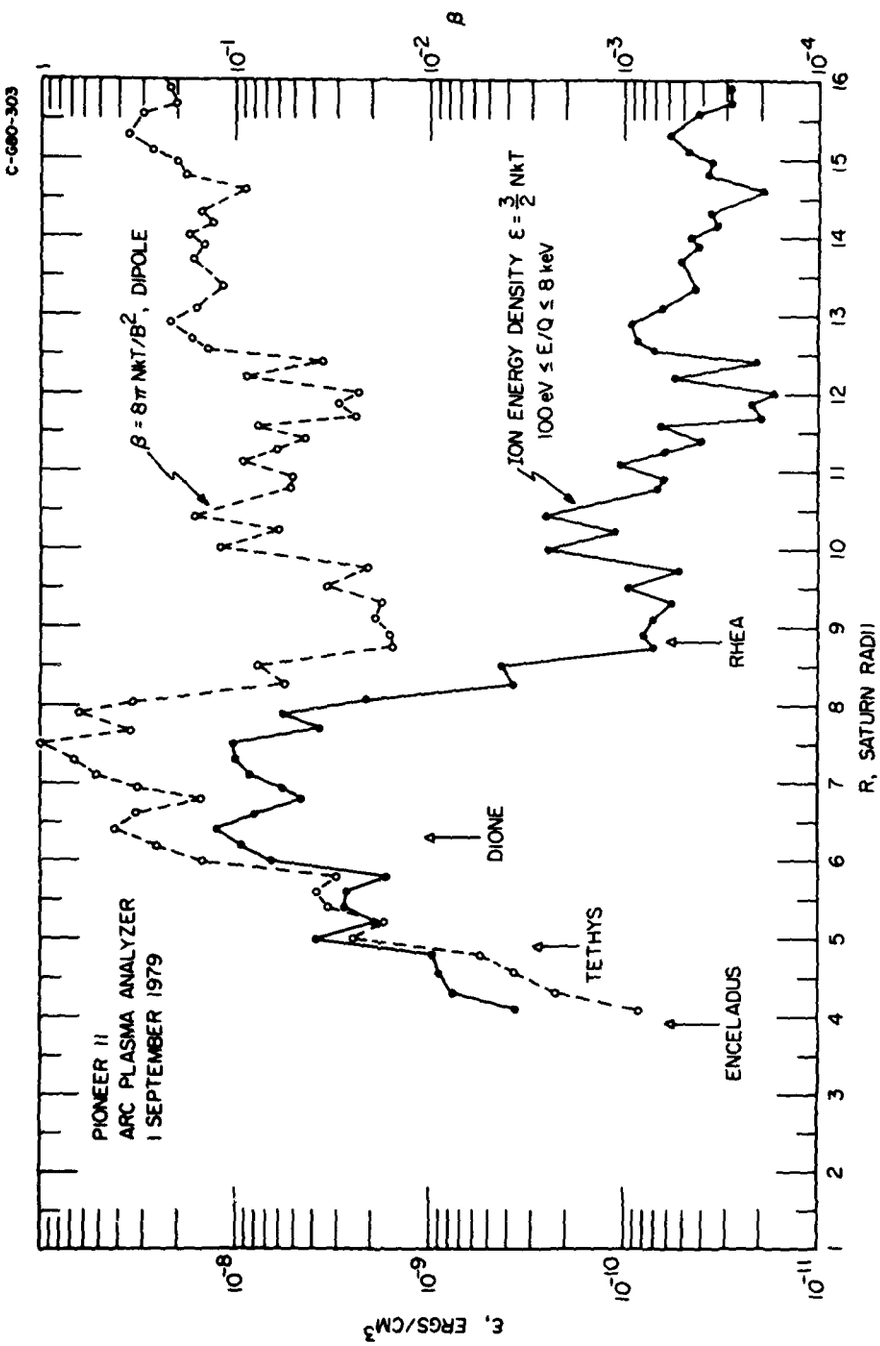
C-680-303
PIONEER 11
ARC PLASMA ANALYZER
1 SEPTEMBER 1979
β = 8π NkT/B², DIPOLE
ION ENERGY DENSITY ε = 3/2 NkT
100 eV ≤ E/Q ≤ 8 keV
DIONE
TETHYS
ENCELADUS
RHEA
β
ε, ERGS/CM³
R, SATURN RADII

Figure 9